Cell Stem Cell

Article

TFEB-mediated endolysosomal activity controls human hematopoietic stem cell fate

Graphical abstract

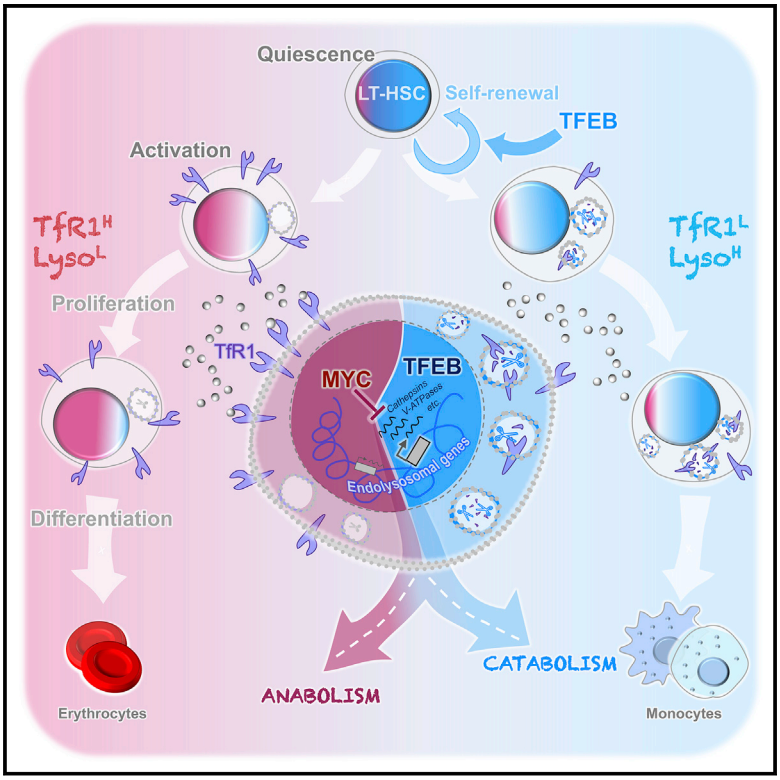

Highlights

- TFEB nuclear localization and lysosomal activity decreases upon LT-HSC activation
- MYC drives LT-HSC metabolic and mitogenic activation and inhibits lysosomal genes
- TFEB induces lysosomal degradation of TfR1, balancing myeloid/erythroid fate choices
- TFEB and lysosomal activity preserve quiescence and enhance self-renewal of LT-HSCs

Authors

Laura García-Prat,
Kerstin B. Kaufmann,
Florin Schneiter, ..., Timm Schroeder,
Stephanie Z. Xie, John E. Dick

Correspondence

sxie@uhnresearch.ca (S.Z.X.),
john.dick@uhnresearch.ca (J.E.D.)

In brief

García-Prat et al. show that lysosomes are regulated dichotomously by TFEB and c-MYC and are crucial for regulating human LT-HSC quiescence, self-renewal, and erythroid/myeloid lineage specification. Anabolic-catabolic lysosomal activity, including endolysosomal degradation of membrane receptors such as TfR1, is required for environmental sensing and activation of LT-HSCs.

García-Prat et al., 2021, Cell Stem Cell *28*, 1–13
November 4, 2021
https://doi.org/10.1016/j.stem.2021.07.003

CellPress

Cell Stem Cell

CellPress
OPEN ACCESS

Article

TFEB-mediated endolysosomal activity controls human hematopoietic stem cell fate

Laura García-Prat,[1,2] Kerstin B. Kaufmann,[1,2] Florin Schneiter,[3] Veronique Voisin,[2,4] Alex Murison,[1,2] Jocelyn Chen,[1,5] Michelle Chan-Seng-Yue,[1,2] Olga I. Gan,[1,2] Jessica L. McLeod,[1,2] Sabrina A. Smith,[1,2] Michelle C. Shoong,[1,2] Darrien Parris,[1,2] Kristele Pan,[1,2] Andy G.X. Zeng,[1,2] Gabriela Krivdova,[1,2] Kinam Gupta,[1,2] Shin-Ichiro Takayanagi,[1,2] Elvin Wagenblast,[1,2] Weijia Wang,[3] Mathieu Lupien,[1,5,6] Timm Schroeder,[3] Stephanie Z. Xie,[1,2,*] and John E. Dick[1,2,6,7,*]

[1]Princess Margaret Cancer Centre, University Health Network, Toronto, ON M5G 1L7, Canada
[2]Department of Molecular Genetics, University of Toronto, Toronto, ON M5S 1A8, Canada
[3]Department of Biosystems Science and Engineering, ETH Zürich, 4058 Basel, Switzerland
[4]The Donnelly Centre, University of Toronto, Toronto, ON M5S 3E1, Canada
[5]Department of Medical Biophysics, University of Toronto, Toronto, ON M5G 1L7, Canada
[6]Ontario Institute for Cancer Research, Toronto, ON M5G 0A3, Canada
[7]Lead contact
*Correspondence: sxie@uhnresearch.ca (S.Z.X.), john.dick@uhnresearch.ca (J.E.D.)
https://doi.org/10.1016/j.stem.2021.07.003

SUMMARY

It is critical to understand how human quiescent long-term hematopoietic stem cells (LT-HSCs) sense demand from daily and stress-mediated cues and then transition into bioenergetically active progeny to differentiate and meet these cellular needs. However, the demand-adapted regulatory circuits of these early steps of hematopoiesis are largely unknown. Here we show that lysosomes, sophisticated nutrient-sensing and signaling centers, are regulated dichotomously by transcription factor EB (TFEB) and MYC to balance catabolic and anabolic processes required for activating LT-HSCs and guiding their lineage fate. TFEB-mediated induction of the endolysosomal pathway causes membrane receptor degradation, limiting LT-HSC metabolic and mitogenic activation, promoting quiescence and self-renewal, and governing erythroid-myeloid commitment. In contrast, MYC engages biosynthetic processes while repressing lysosomal catabolism, driving LT-HSC activation. Our study identifies TFEB-mediated control of lysosomal activity as a central regulatory hub for proper and coordinated stem cell fate determination.

INTRODUCTION

Human long-term hematopoietic stem cells (LT-HSCs), at the apex of the hematopoietic hierarchy, must meet enormous daily demand ($\sim 10^{11}$ cells daily) while sustaining life-long maintenance of the stem cell pool. This hierarchical organization is widely thought to protect LT-HSCs from exhaustion by their maintenance in a quiescent and undifferentiated state, activating only in response to microenvironment signals to generate highly proliferative but more short-lived populations, including short-term HSCs (ST-HSCs) and committed progenitors (Laurenti and Göttgens, 2018). Upon cues to exit this dormant state, HSCs must respond and adapt their metabolism and nutrient uptake to meet increased bioenergetic demands for cell growth and differentiation (Ito et al., 2019). Simultaneously, the events underlying cellular and metabolic activation must also be suppressed in a subset of LT-HSCs to enable re-entry to quiescence, ultimately maintaining the LT-HSC pool through self-renewal (Ito et al., 2019; García-Prat et al., 2017). However, the demand-adapted regulatory circuits of these early steps of hematopoiesis are largely unknown. Sensing signals or nutrient uptake depends on proteins that are embedded in the plasma membrane. These proteins internalize through endocytosis and can be degraded in lysosomes or rerouted back to the cell surface and reused (Palm and Thompson, 2017). Lysosomes are also terminal catabolic stations for autophagy where they clear cytoplasmic components, a process essential for preserving adult stem cell function (Ito et al., 2016; Ho et al., 2017; Xie et al., 2019; García-Prat et al., 2016; Leeman et al., 2018). Recent work shows that lysosomes are not merely degradation stations but also serve as major signaling centers for molecular complex assembly, including mTORC1, AMPK, GSK3, and the inflammasome (Lawrence and Zoncu, 2019). These signaling complexes sense, integrate, and facilitate cross talk between diverse signals and ultimately enable responses such as autophagy, cell growth, membrane repair, and microbe clearance. Although these distinct lysosomal activities have largely been elucidated in cell line models and bulk tissue, they have not been fully investigated in the stem cell context. However, lysosomes in mouse HSCs have been reported to be asymmetrically inherited, predicting future daughter cell fates (Loeffler et al., 2019), and pharmacological inhibition of the lysosomal v-ATPase positively affects

Please cite this article in press as: García-Prat et al., TFEB-mediated endolysosomal activity controls human hematopoietic stem cell fate, Cell Stem Cell (2021), https://doi.org/10.1016/j.stem.2021.07.003

mouse HSC quiescence and engraftment potential (Liang et al., 2020; Ghaffari, 2021). Thus, we hypothesize that lysosomes coordinate the cell cycle and metabolic machinery of LT-HSCs through their ability to sense and respond to diverse signaling cues to adapt their fate and lineage choices.

The MiT/TFE family of transcription factors (TFs) controls lysosomes, with most studies focusing on TFEB as a master regulator of lysosomes. TFEB can sense and respond to stress signals and metabolic cues, including nutrient starvation or mitochondrial damage, by transcriptional activation of endocytosis, autophagy, and lysosomal biogenesis genes (Napolitano and Ballabio, 2016). TFEB and MYC appear to compete for binding to the same chromatin regions in HeLa cells because of a high degree of binding sequence homology (Annunziata et al., 2019), but the biological relevance of this potential competition in a stem cell context has not been determined. MYC regulates many aspects of metabolism and plays a role in murine HSCs by balancing self-renewal and differentiation (Wilson et al., 2004; Laurenti et al., 2008). However, the role of MYC in human HSCs is unknown, and no studies of the role of TFEB in human or mouse HSC function have been undertaken. Here we uncovered MYC-TFEB-mediated dichotomous regulation of lysosomal activity that is required to balance anabolic and catabolic processes that ultimately affect human LT-HSC fate determination.

RESULTS

MYC drives LT-HSC activation by promoting anabolism and inhibiting TFEB-mediated lysosomal activity

During mitogenic activation from quiescence, LT-HSCs enter a transitional state where transcriptional and metabolic changes occur to promote G0 exit with resultant entry into the cell cycle. RNA sequencing (RNA-seq) analysis of uncultured (quiescent LT-HSCs [qLT-HSCs]) versus cultured (activated LT-HSCs [aLT-HSCs]) LT-HSCs sorted from human cord blood (hCB) showed that genes associated with biosynthetic processes, such as ribosome and mitochondrion biogenesis, were the most enriched gene sets in aLT-HSCs (Figure 1A; Figure S1A). This included *MYC* and known MYC targets involved in promoting the cell cycle, protein synthesis, and mitochondrial metabolism (Figure S1B; Figures 1A and 1B; Table S1). Indeed, concordant with mouse HSCs (Cabezas-Wallscheid et al., 2017), MYC protein abundance was barely detectable in qLT-HSCs but increased greatly in aLT-HSCs at 24 and 48 h of *in vitro* culture, when cells are growing in size while still remaining undivided (Laurenti et al., 2015; Figure 1C; Figure S1C). Conversely, autophagy-lysosomal pathway gene sets were among the most upregulated in qLT-HSCs (Figure 1A; Figure S1B; Table S1). Interestingly, *TFEB* gene expression was enriched in qLT-HSCs (Figure 1B). Additionally TFEB, a protein typically only showing nuclear localization upon stress (Puertollano et al., 2018), was found to be nuclear in qLT-HSCs (Figures 1B and 1C; Figure S1D). In contrast, TFEB levels and nuclear localization were reduced in aLT-HSCs (Figure 1C). Other MiT/TFE family members were not expressed with the same trajectories across the human hematopoietic hierarchy (Figures S1E and S1F). Importantly, of the two MiT/TFE family members that bind to genetic elements of the CLEAR network (TFEB and TFE3) (Martina et al., 2014) and show nuclear localization, only TFEB changes to cytoplasmic localization upon activation (Figures S1G–S1I). MYC and TFEB expression anticorrelated at the single-cell level (Figure 1D). LAMP1 staining revealed that aLT-HSCs had expanded lysosomal mass compared with qLT-HSCs (Figure 1C). However, TFEB and genes involved in lysosome activity have been found to be downregulated during LT-HSC activation, suggesting that this increased lysosomal content may be due to decreased lysosomal turnover (Luzio et al., 2014; Mutvei et al., 2020). We validated this idea by blocking lysosome acidification and degradation with short-term bafilomycin (BAF) treatment; qLT-HSC had higher accumulation of lysosomes compared with aLT-HSCs (Figure 1E; Figure S2A). In agreement, aLT-HSCs displayed a gradual decrease in lysosomal acidification, indicating fewer functional lysosomes (Figure S2B), and longer exposure to BAF (48 h) significantly decreased qLT-HSC viability but did not affect aLT-HSCs (Figures S2C and S2D).

To directly assess MYC function in LT-HSC activation, we transduced LT-HSC with a MYC-overexpressing lentivirus (LV) (MYC^{WT}-OE) (Figure 1F). MYC^{WT}-OE LT-HSCs expanded ~3-fold more than control cells; 6 days after transduction, they exhibited increased mitochondrial mass and expression of anabolic genes involved in ribosome biogenesis, protein translation, mitochondrial metabolism, and MYC target genes (Figures 1G–1I; Figures S2E and S2F; Table S1). Conversely, 4 days of MYC inhibition (Cabezas-Wallscheid et al., 2017) restrained LT-HSC activation, as demonstrated by reduced mitochondrial mass, ROS production, and more G0-quiescent cells (Figures S2G and S2H). MYC^{WT}-OE downregulated lysosome-related genes, consistent with our observation that lysosomal degradation is reduced in aLT-HSCs (Figure 1H,I). Importantly, MYC inhibition increased TFEB nuclear localization and lysosomal activity, which was blunted by *TFEB* knockdown (shTFEB) (Figures 1J and 1K). In line with these results, we detected MYC binding at the promoters of TFEB targets (Palmieri et al., 2011) in several cell lines (Figure S2I), whereas we could not detect enrichment of TFEB binding at promoters of MYC targets in hCB cells (Figure S2J). This suggests that, by binding to promoters of TFEB-regulated genes, MYC denies promoter occupancy to TFEB and thereby suppresses expression of TFEB targets, as shown previously in HeLa cells (Annunziata et al., 2019). Our data show that TFEB is high in quiescent LT-HSCs and that, when MYC is upregulated upon *in vitro* mitogenic stimulation, it causes repression of TFEB-associated lysosomal programs, driving LT-HSC activation and anabolism.

TFEB regulates lysosomal degradation of environment-sensing receptors in LT-HSCs

To gain insight into how TFEB regulates the transition from quiescence to activation, we performed transcriptomics analysis of control (CTRL) and wild-type TFEB overexpression ($TFEB^{WT}$ OE LT-HSCs (Figure 2A; Figures S2K and S2L). As expected for a transcriptional activator, 67 of 68 differentially expressed genes were upregulated in $TFEB^{WT}$ OE compared with CTRL LT-HSCs (Figure S2L; Table S2). Lysosome-related gene sets were the most significantly enriched, including 14 different V-ATPase subunits that are required for lysosome and endosome acidification as well as cargo degradation (Figures 2B and 2C; Figure S2M; Table S2). Moreover, endosome transit to

Please cite this article in press as: García-Prat et al., TFEB-mediated endolysosomal activity controls human hematopoietic stem cell fate, Cell Stem Cell (2021), https://doi.org/10.1016/j.stem.2021.07.003

CellPress
OPEN ACCESS

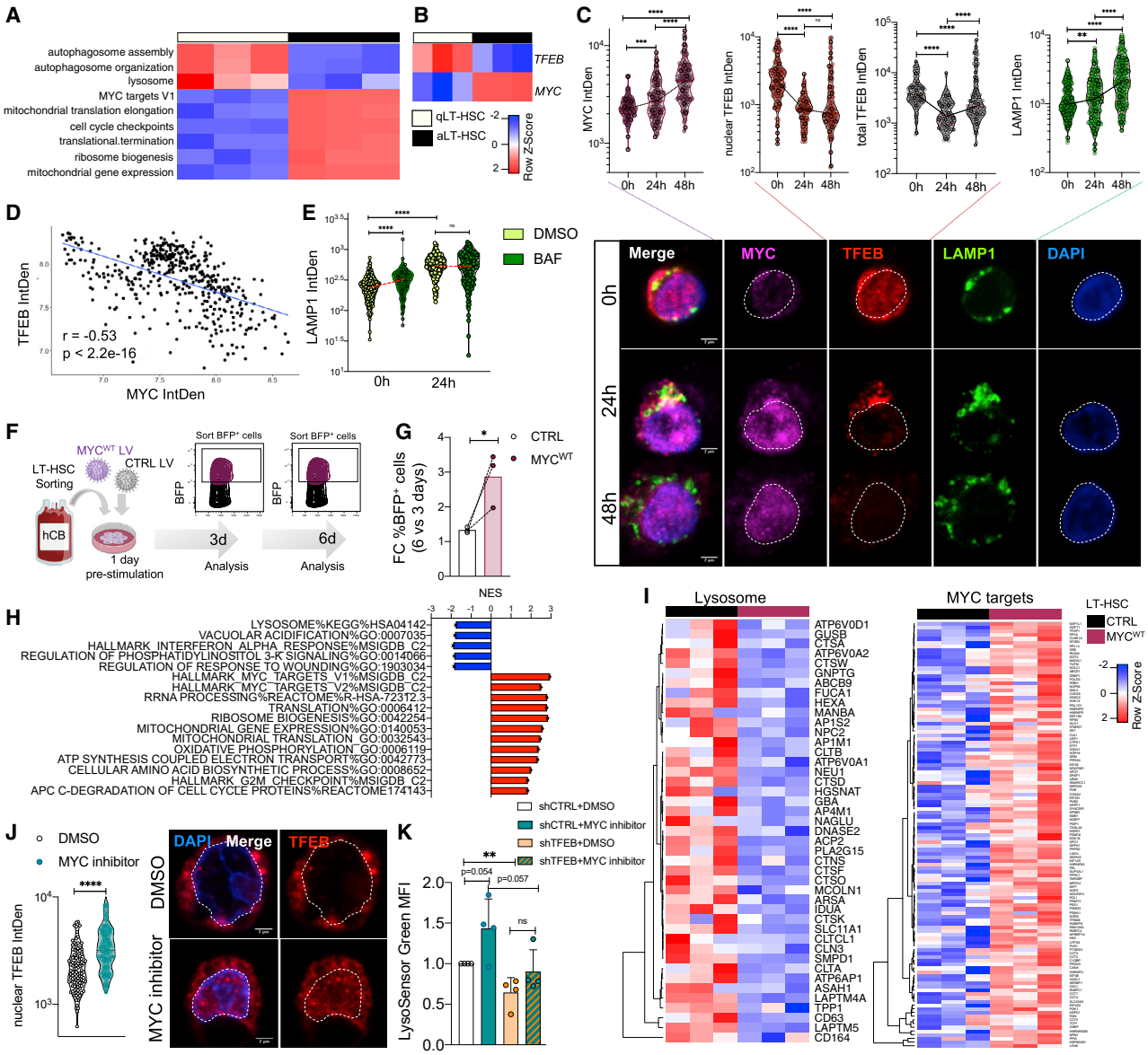

Figure 1. MYC drives LT-HSC activation by promoting anabolism and inhibiting lysosomal activity

(A) RNA-seq analysis of qLT-HSCs versus cultured LT-HSCs for 4 days (aLT-HSCs). n = 3 CB.

(B) *MYC* and *TFEB* expression in LT-HSCs from (A).

(C) Confocal analysis of TFEB, MYC, and LAMP1 in qLT-HSCs and cultured LT-HSCs for 24 h or 48 h. IntDen, integrated density. Scale bar, 2 μm. n = 3 CB, 469–867 cells/staining. Mann-Whitney test.

(D) Correlation of normalized IntDen values for MYC and TFEB from (C).

(E) Confocal analysis of LAMP1 in quiescent or 24-h-cultured LT-HSCs treated with DMSO or BAF for 3 h. Mann-Whitney test. n = 3 CB, 594 cells.

(F) Scheme for LT-HSCs transduced with an LV expressing BFP (blue fluorescent protein) and CTRL or MYC^{WT} genes. BFP^+ cells were sorted at 3 or 6 days for analysis.

(G) % BFP^+ LT-HSCs from (F) quantified by flow cytometry 6 versus 3 days after transduction. n = 3 CB. FC, fold change.

(H) RNA-seq analysis of LT-HSCs from (F) 6 days after transduction and normalized enrichment score (NES) of pathways differentially enriched in MYC^{WT} versus CTRL LT-HSCs by gene set enrichment analysis (GSEA). False discovery rate (FDR) $q \leq 0.05$. n = 3 CB.

(I) Expression of the indicated genes in LT-HSCs from (F).

(J) Confocal analysis of TFEB in LT-HSCs treated for 4 days with DMSO or MYC inhibitor. n = 3 CB, 272 cells. Mann-Whitney test.

(K) LysoSensor mean fluorescence intensity (MFI) of LT-HSCs transduced with an LV expressing mCherry and a shRNA against *Renilla* (shCTRL) or TFEB (shTFEB) treated with DMSO or MYC inhibitor from 1–5 days after transduction. n = 4 CB.

*p < 0.05, **p < 0.01, ***p < 0.001, ****p < 0.0001. Unpaired t test unless otherwise indicated. See also Table S1 and Figures S1 and S2.

Please cite this article in press as: García-Prat et al., TFEB-mediated endolysosomal activity controls human hematopoietic stem cell fate, Cell Stem Cell (2021), https://doi.org/10.1016/j.stem.2021.07.003

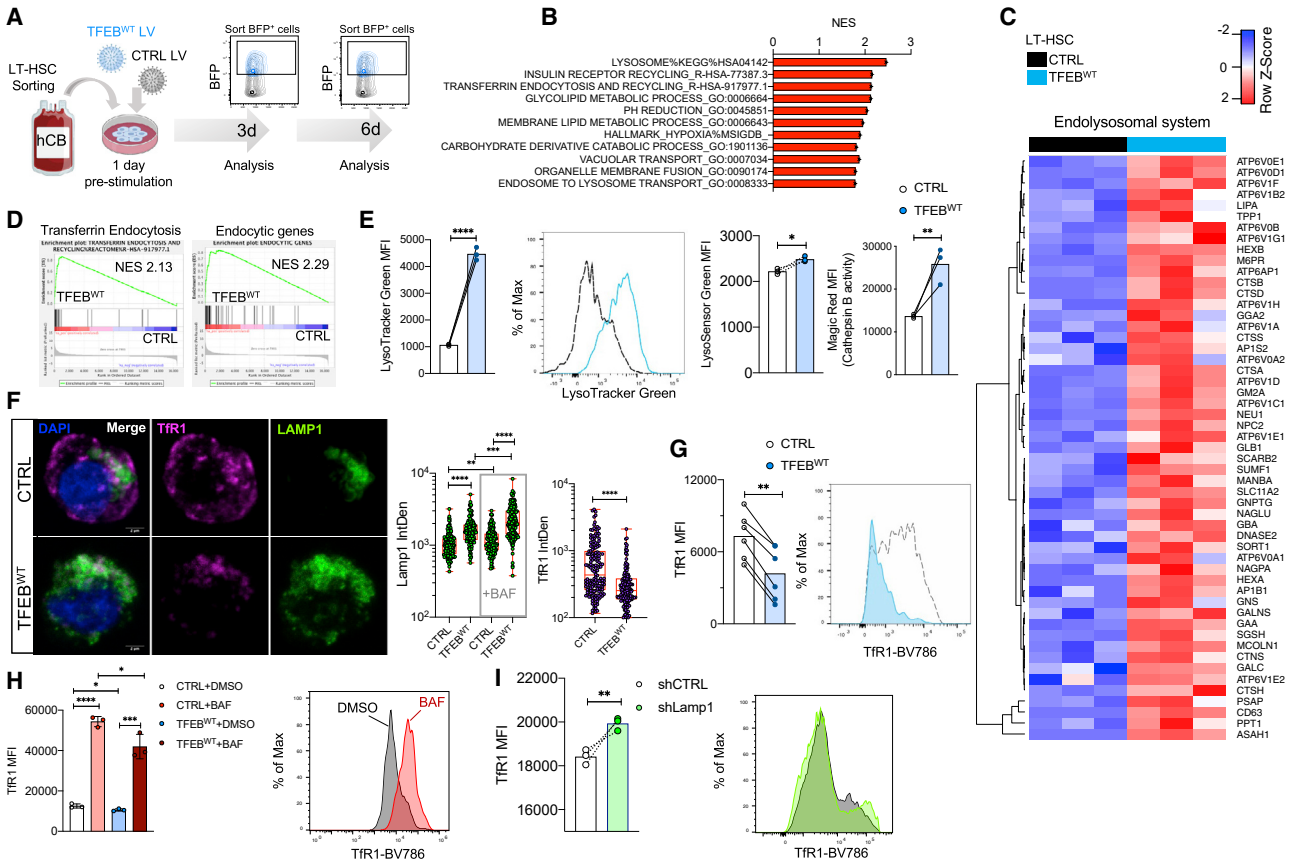

Figure 2. TFEB regulates lysosomal degradation of environment-sensing receptors

(A) Scheme of LT-HSCs transduced with an LV expressing BFP and CTRL (GP91) or TFEB^{WT} genes. BFP^{+} cells were sorted for analysis at 3 or 6 post-transduction.

(B) RNA-seq analysis of LT-HSCs from (A) 3 days after transduction and NES value of pathways positively enriched in TFEB^{WT} versus CTRL LT-HSCs by GSEA. FDR q $\leq$ 0.05. n = 3 CB.

(C) RNA-seq expression of endolysosomal genes in LT-HSCs from (A).

(D) GSEA plots of indicated gene sets in LT-HSCs from (A). FDR q $\leq$ 0.05.

(E) LT-HSCs from (A) stained with LysoTracker, LysoSensor, and Magic Red (Cathepsin B activity) and analyzed by flow cytometry 6 days after transduction. n = 3 CB.

(F) Confocal analysis of LAMP1 and TfR1 in LT-HSCs from (A) treated for 3 h with BAF or DMSO, 6 days after transduction. Scale bar, 2 μm. n = 3 CB, 635 cells. Mann-Whitney test.

(G) TfR1 MFI analyzed by flow cytometry in LT-HSCs from (A). Paired t test.

(H) TfR1 MFI analyzed by flow cytometry in CTRL and TFEB^{WT} OE LT-HSCs treated with DMSO or BAF from 1–5 days after transduction. n = 3 CB.

(I) Sorted LT-HSCs were cultured for 1 day prior to transduction with lentiviral vectors expressing mCherry and shCTRL or shLAMP1. mCherry^{+} cells were sorted at 3 days, and TfR1 MFI was analyzed by flow cytometry. n = 3 CB. Paired t test.

*p < 0.05, **p < 0.01, ***p < 0.001, ****p < 0.0001. Unpaired t test unless otherwise indicated. See also Tables S1 and S2 and Figures S2 and S3.

lysosomes or receptor endocytosis genes (such as transferrin or insulin receptor) were upregulated concurrently, indicating overall induction of the endolysosomal pathway (Figures 2B–2D). ATAC-seq profiling uncovered 116 sites uniquely acquired in TFEB^{WT} OE versus 438 sites uniquely acquired in control LT-HSCs (Table S2). TF recognition motif analysis identified specific E-boxes recognized by the MITF family of TFs as the most enriched binding motif in open chromatin regions gained upon TFEB^{WT} OE, whereas no significantly enriched motifs were found in CTRLs (Figures S2N and S2O). Genes whose promoters fell within these gained elements showed enriched expression in TFEB^{WT} OE LT-HSCs but depletion in shTFEB LT-HSCs relative to CTRLs (Figure S2P). Moreover, the promoters of those genes upregulated in TFEB OE LT-HSCs were enriched for TFEB binding in chromatin immunoprecipitation sequencing (ChiP-seq) analysis of hCB cells (Figure S2J), providing strong evidence that the observed transcriptional changes are mediated directly by TFEB binding events (Figure S2P). As expected, TFEB^{WT} OE increased LT-HSC lysosomal activity compared with CTRLs, as demonstrated by the higher number, acidification, and turnover of lysosomes as well as higher Cathepsin expression and activity (Figures 2E and 2F; Figures S2Q and S3A). Notably, membrane protein levels of transferrin receptor 1 (TfR1), which is required for iron-bound transferrin uptake through clathrin-mediated endocytosis, were reduced significantly reduced in TFEB^{WT} OE cells despite only mild changes in levels of *TFRC*

Please cite this article in press as: García-Prat et al., TFEB-mediated endolysosomal activity controls human hematopoietic stem cell fate, Cell Stem Cell (2021), https://doi.org/10.1016/j.stem.2021.07.003

CellPress
OPEN ACCESS

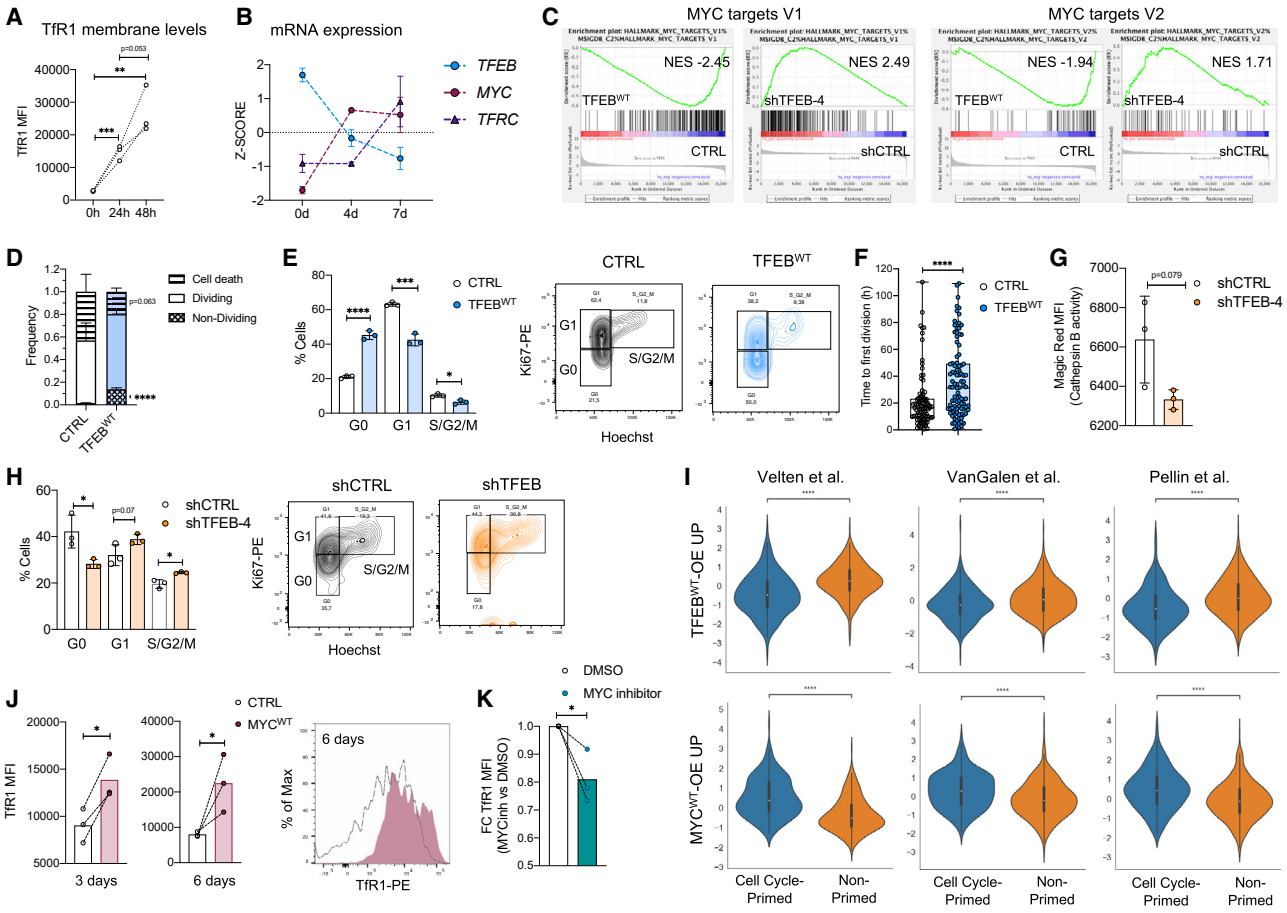

Figure 3. TFEB-induced endolysosomal degradation inhibits c-MYC-driven anabolic processes and promotes LT-HSC quiescence

(A) TfR1 MFI analyzed by flow cytometry in qLT-HSCs and cultured LT-HSCs for 24 and 48 h. n = 3 CB.

(B) RNA-seq expression of *TFRC*, *MYC*, and *TFEB* in CTRL LT-HSCs at the indicated time points. n = 3 CB.

(C) GSEA plots of the indicated gene sets in LT-HSCs from Figure 2A and Figure S3L. FDR q $\leq$ 0.05.

(D) Distribution of cell fate by time-lapse imaging analysis from 3 to 6 days after transduction of LT-HSCs from Figure 2A. n = 3 CB. Mann-Whitney test.

(E) Cell cycle analysis of LT-HSCs from Figure 2A, 6 days after transduction. n = 3 CB.

(F) Time to first division analysis of LT-HSCs from Figure 2A from 3 to 6 days after transduction in hours. Mann-Whitney test. n = 3 CB, 192 cells.

(G) Sorted LT-HSCs were cultured for 1 day prior to transduction with lentiviral vectors expressing mCherry and shCTRL or shTFEB. mCherry$^+$ cells were sorted at 3 days and stained with Magic for flow cytometry analysis. n = 3 CB.

(H) Cell cycle analysis of LT-HSCs from (G), 3 days after transduction. n = 3 CB.

(I) Graphs showing the enrichment score of MYC^{WT} OE- and TFEB^{WT} OE-upregulated genes (FDR q $\leq$ 0.05) in 3 single-cell RNA-seq datasets (Velten et al., 2017; van Galen et al., 2019; Pellin et al., 2019). For more information on how the cell-cycle-primed and non-primed cell clusters were identified, see STAR Methods (Xie et al., 2019).

(J) TfR1 MFI analyzed by flow cytometry in LT-HSCs from Figure 1F 3 and 6 days after transduction. n = 3 CB. Paired t test.

(K) FC in TfR1 membrane levels analyzed by flow cytometry in LT-HSCs cultured for 4 days with DMSO or MYC inhibitor. n = 3 CB.

*p < 0.05, **p < 0.01, ***p < 0.001, ****p < 0.0001. Unpaired t test unless otherwise indicated. See also Tables S1 and S2 and Figures S3 and S4.

mRNA (Figure 2G; Figure S3B). Confocal analysis confirmed the reduction of TfR1 membrane levels upon TFEB OE and demonstrated the existence of TfR1$^+$/LAMP1$^+$ late endosomes/lysosomes (Figure 2F; Figures S3A and S3C). BAF treatment, shown previously to block TfR1 trafficking to late endosomes/lysosomes (Cao et al., 2016), or *LAMP1* knockdown (shLAMP1) resulted in increased TfR1 membrane levels that could not be rescued by TFEB^{WT} OE (Figures 2H and 2I; Figure S3D). Thus, we can conclude that TFEB induces clearance of TfR1 from the membrane of LT-HSCs through endolysosomal degradation.

TFEB-induced lysosomal activity inhibits MYC-driven anabolic processes and promotes LT-HSC quiescence

We hypothesized that TFEB-induced endolysosomal degradation of cell surface receptors such as TfR1 is required to maintain LT-HSC quiescence and that inhibition of this pathway could lead to enhanced TfR1 membrane levels and LT-HSC activation. Although qLT-HSCs were mostly negative for TfR1, increased TfR1 membrane expression correlated with *MYC* elevation and preceded upregulation of *TFRC* mRNA levels during LT-HSC activation (Figures 3A and 3B). Transcriptomics analysis showed large and consistent downregulation of gene sets involved in cell

Please cite this article in press as: García-Prat et al., TFEB-mediated endolysosomal activity controls human hematopoietic stem cell fate, Cell Stem Cell (2021), https://doi.org/10.1016/j.stem.2021.07.003

cycle regulation, RNA processing/transport, and ribosome biogenesis upon TFEB^{WT} OE (Figure 3C; Figures S3E–S3G; Table S2). This group of anabolic genes included *MYC* and MYC target genes, and its downregulation correlated with lower levels of mitochondria and ROS (Figure 3C; Figures S3E–S3H), indicating that TFEB maintains LT-HSCs in a low metabolic state during culture. TFEB^{WT} OE restricted LT-HSC division over 6 days of time-lapse imaging compared with CTRLs, and cells remained Ki67 and EdU negative in flow cytometry analyses (Figures 3D and E; Figures S3I and S3J), indicating that TFEB^{WT} OE inhibits LT-HSC quiescence exit. Furthermore, single-cell tracking of TFEB^{WT} OE LT-HSCs showed delayed division kinetics among dividing cells relative to CTRL, resulting in overall reduced cellular expansion (Figure 3F; Figure S3I; Video S1). Induction of this quiescent/low metabolic state upon TFEB^{WT} OE also protected LT-HSCs from cell death during *in vitro* culture (Figure 3D). Importantly, BAF treatment decreased TFEB^{WT} OE LT-HSC viability compared with CTRL LT-HSCs (Figure S2D), similar to qLT-HSCs (Figure S2C), indicating that the beneficial effects of TFEB OE on LT-HSCs are mediated by increasing lysosomal function.

In contrast to TFEB^{WT} OE, shTFEB resulted in decreased lysosomal and Cathepsin B activity and higher expression of anabolic pathways and increased numbers of cycling cells (Figures 1K, 3C, 3G, and 3H; Figures S3F, S3G, S3K, and S3L; Table S1). Indeed, the transcriptomics programs upregulated by shTFEB and MYC^{WT} OE in LT-HSCs were highly concordant (Figure S3G). In agreement, genes upregulated by TFEB^{WT} OE and downregulated by MYC^{WT} OE were enriched in qLT-HSCs and in single-cell RNA-seq subsets of bone marrow hematopoietic stem and progenitor cells classified as more dormant (non-primed) (Xie et al., 2019; Velten et al., 2017; Pellin et al., 2019; van Galen et al., 2019; Figure 3I; Figure S4A). Moreover, LT-HSCs exhibited increased cell surface levels of TfR1 without significant changes in *TFRC* mRNA levels upon MYC^{WT} OE, whereas MYC inhibition reduced surface expression of TfR1, consistent with the observed MYC-directed repression of the endolysosomal pathway (Figures 1I, 3J, and 3K; Figure S3B). Importantly, *TFRC* knockdown (shTFRC) reduced Ki67^{+} LT-HSCs during culture, indicating that TfR1 is instrumental for LT-HSC activation (Figures S4B and S4C). Overall, our findings demonstrate that TFEB suppresses MYC activation and restrains a MYC-driven anabolic program while inducing endolysosomal degradation of membrane receptors such as TfR1, maintaining a quiescent, low metabolic state in LT-HSCs.

Lysosomal activity governs LT-HSC lineage specification

Because TfR1 is required for erythropoiesis (Moura et al., 2015), we next examined whether lysosomal activity differs among subpopulations of LT-HSCs with distinct TfR1 membrane levels and whether this correlates with differing lineage commitment potential. LT-HSCs, sorted on the basis of higher (Lyso^{H}) lysosomal activity in culture, were reminiscent of TFEB^{WT} OE LT-HSCs because they displayed higher acidification and levels of Cathepsin B activity and lower TfR1 surface expression levels than LT-HSCs with low activity (Lyso^{L}) (Figures 2E–2G and 4A; Figures S4D and S4E). Colony-forming cell (CFC) assays showed that the cloning efficiency was significantly higher from Lyso^{L} than Lyso^{H} LT-HSC, predominantly because of increased BFU-Es (burst-forming units-erythroid), although total cellular output was unchanged (Figures 4B–4D; Figure S4F). The percentage and total number of cells expressing the erythroid marker GlyA and/or TfR1 were reduced in the progeny of Lyso^{H} compared with Lyso^{L} LT-HSC, whereas Lyso^{H} LT-HSCs showed increased myeloid differentiation potential (CD33^{+}/CD15^{+}cells) (Figures 4C and 4D; Figure S4G). Similarly, single-cell stromal (SCS) assays showed that myeloid and erythroid differentiation are associated with higher and lower lysosomal activity, respectively (Figures S4H–S4K). Thus, the levels of lysosomal activity are inversely correlated with TfR1 surface expression levels and are tied to LT-HSC erythroid-myeloid lineage fate choices.

We wanted to find out whether similar regulation of TfR1-lysosomal degradation by TFEB and MYC might occur as part of the typical sequence of events that occurs during lineage commitment of LT-HSCs. Interestingly, the gene expression patterns of *TFEB* and *MYC* in subpopulations downstream of LT-HSCs were also mutually exclusive: megakaryocyte-erythrocyte progenitors (MEPs) had low *TFEB* and high *MYC* expression, whereas granulocyte-monocyte progenitors (GMPs) exhibited the inverse expression pattern (Figure 4E). TfR1 membrane levels were higher in MEPs, correlating with *MYC* and anti-correlating with *TFEB* expression (Figures 4E and 4F). Analysis of more mature populations revealed that *TFEB* was distinctly suppressed in erythroid progenitors (Figure S4L).

To determine functionally whether the lysosomal program is instrumental in regulating the erythroid/myeloid commitment of LT-HSCs, we assessed LT-HSC differentiation potential after modulation of TFEB expression. TFEB^{WT} OE in LT-HSCs caused a complete block of erythroid differentiation, as demonstrated by an almost complete absence of BFU-E colonies and GlyA^{+} cells in CFC and SCS assays; similar results occurred in ST-HSCs upon TFEB^{WT} OE (Figures 4G and 4H; Figures S4M–S4T). shTFEB or shLAMP1 in LT-HSCs produced the opposite phenotype (Figures S4U–S4X and S5A). Importantly, shTfR1 also reduced BFU colony formation, similar to TFEB^{WT} OE in LT-HSCs, demonstrating that TfR1 is important for early erythroid commitment (Figure 4I; Figure S5B). Remarkably, TFEB^{WT} OE in committed MEP subpopulations (F1, F2/F3) (Notta et al., 2016) was sufficient to suppress TfR1 membrane levels and abolish their erythroid potential while slightly increasing their myeloid output in CFC and SCS assays (Figures 4J and 4K; Figures S1A and S5C–S5L). Transcriptomic analysis of TFEB^{WT} OE MEP F2/3 subsets confirmed that TFEB imposes a myeloid-associated gene program and inhibits the expression of key TFs essential for erythrocyte and megakaryocyte differentiation, such as GATA1 or RUNX1 (Figures S5M–S5P and S6A; Table S1). Thus, TFEB expression is sufficient to alter erythroid-myeloid fate decisions even in a progenitor subpopulation committed to erythropoiesis and provides strong evidence that TFEB-mediated induction of the endolysosomal pathway controls early lineage determination in LT-HSC as well as downstream progenitors.

To determine whether TFEB may exert its functions through mechanisms other than transcriptional activation, we overexpressed TFEB^{WT} or a TFEB variant unable to activate transcription because of disruption of its DNA binding domain (TFEB$^{H240R-I243N}$) in hCB CD34^{+}CD38^{-} cells (Figures S6B–S6E).

Please cite this article in press as: García-Prat et al., TFEB-mediated endolysosomal activity controls human hematopoietic stem cell fate, Cell Stem Cell (2021), https://doi.org/10.1016/j.stem.2021.07.003

CellPress
OPEN ACCESS

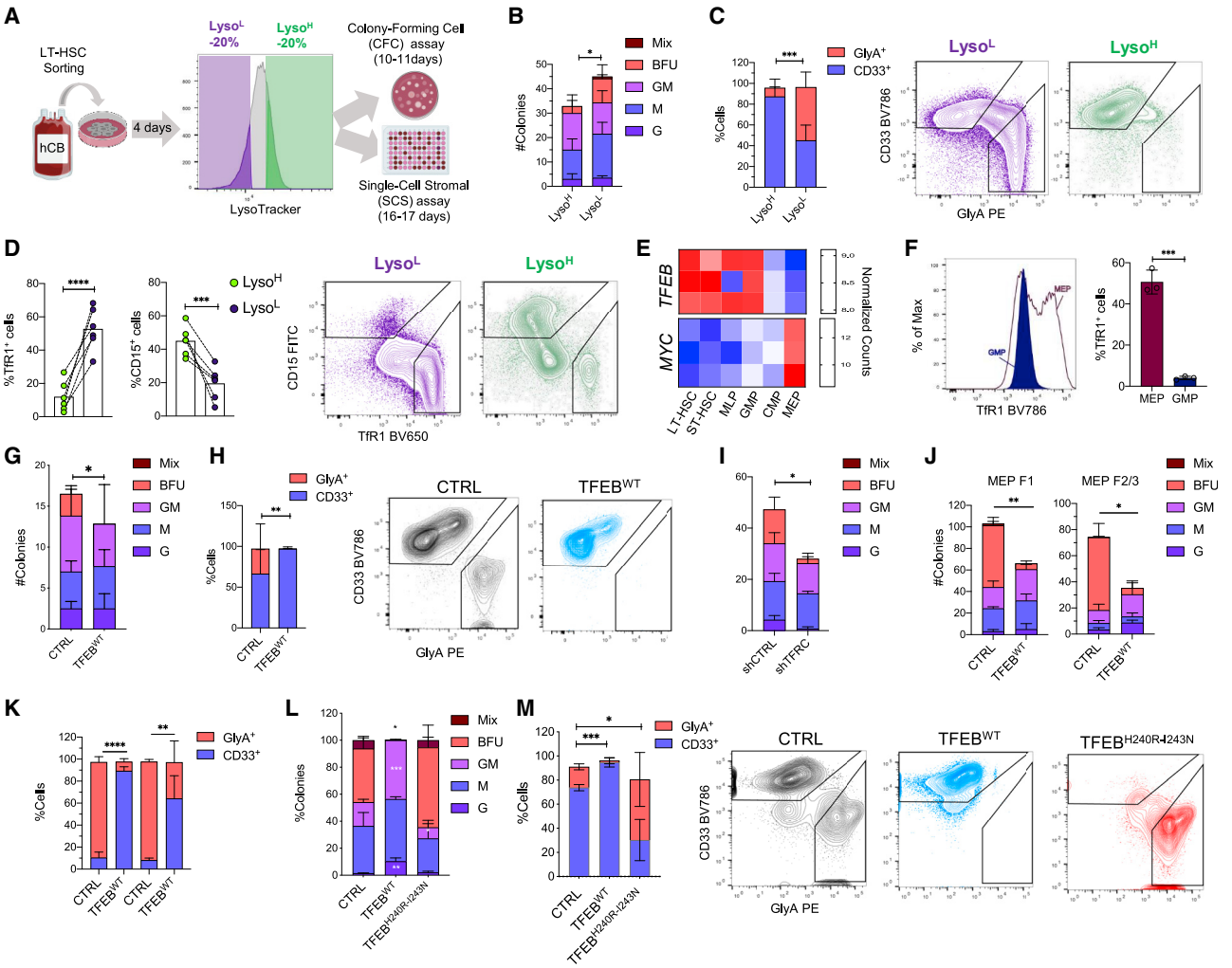

Figure 4. Lysosomal activity governs LT-HSC lineage specification

(A) Experimental scheme. LT-HSCs were cultured for 4 days, stained with LysoTracker, and sorted for the indicated differentiation assays.

(B–D) CFC colony distribution for LT-HSCs from (A) scored under the microscope and GlyA$^+$ and CD33$^+$ lineage analysis by flow cytometry after 10 days of plating. n = 3 CB.

(E) RNA-seq normalized counts for *TFEB* and *MYC* in the indicated cell populations sorted as in Figure S1A. n = 3 CB.

(F) TfR1 membrane expression analysis in MEP and GMP cells after 4 days in culture. n = 3 CB.

(G and H) LT-HSCs from Figure S4M were plated for the CFC assay as in (B) and (C). n = 3 CB.

(I) Sorted LT-HSCs were cultured for 1 day prior to transduction with lentiviral vectors expressing mCherry and shCTRL or shTFRC. mCherry$^+$ cells were sorted at 6 days for CFC assays as in (B) and (C). n = 3 CB.

(J and K) MEP F1 and MEP F2/3 were sorted from CD34-enriched hCB following the sorting scheme displayed in Figure S1A and cultured for 1 day prior to transduction with an LV expressing BFP and one of the following genes: CTRL or TFEB^{WT}. BFP$^+$ cells were sorted at 3 days and plated for the CFC assay as in (B) and (C). n = 3 CB.

(L and M) CFC assay with CD34$^+$CD38$^-$ cells from Figure S6C as in (B) and (C). n = 4 CB. *p < 0.05, **p < 0.01, ***p < 0.001, ****p < 0.0001. Unpaired t test unless otherwise indicated.

See also Tables S1 and S2 and Figures S4–S6.

Flow cytometry analysis showed that OE of TFEB^{WT} but not TFEB$^{H240R\text{-}I243N}$ increased autophagosome/lysosome formation and restrained expansion of CD34$^+$CD38$^-$ cells *in vitro* (Figures S6F and S6G). In CFC assays, TFEB^{WT} strongly inhibited erythroid commitment and enhanced myeloid differentiation, whereas TFEB$^{H240R\text{-}I243N}$ expression produced the opposite effect (Figures 4L and 4M). These results indicate that TFEB exerts its functions primarily through transcriptional activation. We speculated that TFEB$^{H240R\text{-}I243N}$ acts in a dominant-negative manner, perhaps through formation of homodimers sequestering other TFEB molecules. These results independently support our findings with TFEB^{WT} OE and establish that TFEB-mediated induction of lysosomal activity is required for myelopoiesis but is incompatible with erythroid differentiation. Our study has uncovered lysosomes as transcriptionally controlled central signaling hubs that govern lineage determination.

Please cite this article in press as: García-Prat et al., TFEB-mediated endolysosomal activity controls human hematopoietic stem cell fate, Cell Stem Cell (2021), https://doi.org/10.1016/j.stem.2021.07.003

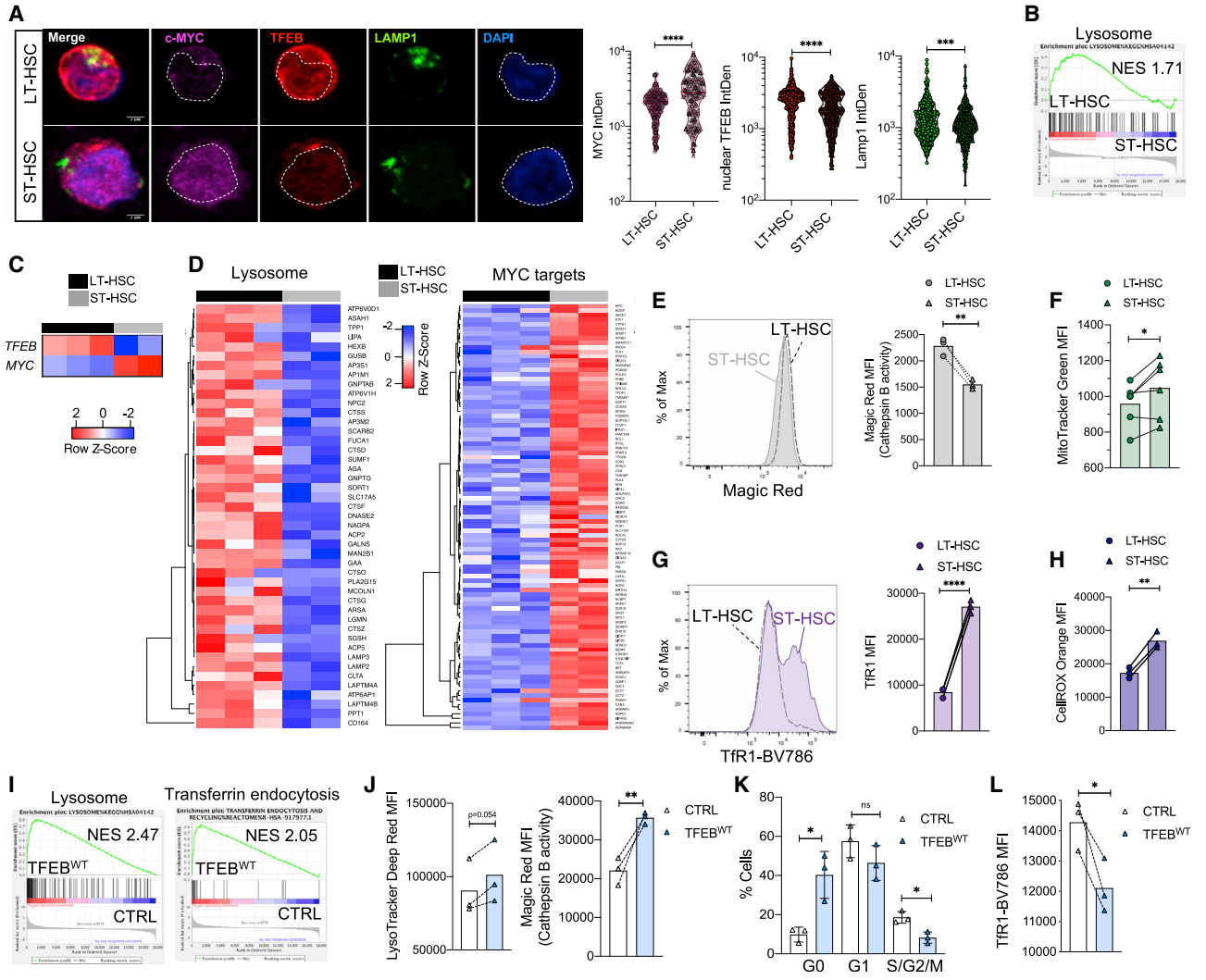

Figure 5. Enhanced TFEB-driven lysosomal activity differentiates LT- from ST-HSCs

(A and B) Confocal analysis of LT-HSCs and ST-HSCs stained for TFEB, LAMP1, MYC, and DAPI. Scale bar, 2 μm. n = 3 CB, 239–951 individual cells/staining. Mann-Whitney test.

(C and D) RNA-seq expression of the indicated genes in LT- and ST-HSCs cultured for 4 days. n = 2–3 CB.

(E–H) Magic Red, TfR1, MitoTracker, and CellROX MFI in LT- and ST-HSCs cultured for 4 days and analyzed by flow cytometry. n = 3–6 CB. Paired t test.

(I) ST-HSCs transduced with lentiviral vectors expressing BFP and CTRL or TFEB^{WT} genes. BFP^{+} cells were sorted at 3 and 6 days for the different analyses. RNA-seq analysis was performed 3 days after transduction. GSEA plots of the indicated gene sets are shown. n = 2 CB.

(J) LysoTracker and Magic Red analyzed by flow cytometry in ST-HSCs from (I). n = 3 CB.

(K) Cell cycle analysis of ST-HSCs from (I). n = 3 CB.

(L) TfR1 MFI analyzed by flow cytometry on ST-HSCs from (I). n = 3 CB.

*p < 0.05, **p < 0.01, ***p < 0.001, ****p < 0.0001. Unpaired t test unless otherwise indicated. See also Table S1 and Figure S6.

Enhanced TFEB-driven lysosomal activity distinguishes LT-HSCs from ST-HSCs

ST-HSCs are the immediate downstream progeny of LT-HSCs and share many transcriptional and functional properties. However, they differ in their quiescence exit kinetics and self-renewal properties (Laurenti et al., 2015). Because our data indicate that TFEB imposes a metabolically low quiescent state in LT-HSCs and restrains their expansion while inducing endolysosomal degradation of specific membrane receptors, we hypothesized that the TFEB-controlled lysosomal program could be differentially regulated in LT- versus ST-HSCs. In relation to qST-HSCs, qLT-HSCs showed transcriptional enrichment of lysosomal pathway genes and contained variable but overall higher levels of lysosomes (Figures 5A and 5B; Figure S6H; Table S1). The observed enrichment of lysosomal genes was associated with higher levels of nuclear TFEB and lower levels of MYC in qLT- versus qST-HSCs (Figure 5A). In short-term cultures, aLT-HSCs also showed enrichment of *TFEB* and lysosomal genes with depletion of *MYC* and its target genes in comparison with aST-HSCs (Figures 5C and 5D; Figure S6I; Table S1). Consistent with these transcriptomics results, aLT-HSCs exhibited enhanced lysosomal activity as defined by Cathepsin B

Please cite this article in press as: García-Prat et al., TFEB-mediated endolysosomal activity controls human hematopoietic stem cell fate, Cell Stem Cell (2021), https://doi.org/10.1016/j.stem.2021.07.003

activity and reduced levels of mitochondria, ROS, and TfR1 compared with aST-HSCs (Figures 5E–5H). TFEB^{WT} OE in ST-HSCs induced a transcriptional program similar to that of LT-HSCs with enrichment of endolysosomal genes and depletion of cell cycle- and biosynthesis-related genes (Figure 5I; Figures S6J and S6K; Table S1). Functionally, TFEB OE in ST-HSCs induced lysosomal activity with inhibition of quiescence exit and reduction in TfR1 membrane levels (Figures 5J–5L; Figure S6L). MYC inhibition suppressed mitogenic and metabolic activation of ST-HSCs in culture (Figure S6M). Thus, aspects of an LT-HSC-specific program can be imposed on ST-HSCs upon ectopic TFEB expression or MYC inhibition. These findings indicate that an enhanced TFEB-regulated lysosomal program distinguishes LT- from ST-HSCs and actively restrains the anabolic processes of LT-HSCs with resultant limitation of their cellular output upon mitogenic activation.

TFEB-regulated lysosomal activity controls LT-HSC self-renewal

We next investigated whether enhanced lysosomal activity in LT-HSCs affected self-renewal, the hallmark trait of stem cells. TFEB^{WT} OE in LT-HSCs resulted in an initial decrease but subsequent increase in total colonies and cells in serial re-plating CFC assays (Figures 6A and 6B). In contrast, shTFEB blunted LT-HSC self-renewal ability in secondary CFC assays, prompting us to directly assess LT-HSC self-renewal capacity using gold-standard xenograft assays (Figure 6C). CD34^{+}CD38^{-} hCB cells transduced with a TFEB^{WT} OE lentiviral vector generated significantly smaller grafts in *NOD.Cg-Prkdcscidll2rgtm1Wjl/SzJ* (NSG) and NSG-W41 mice at 4 and 17 weeks compared with CTRLs, in keeping with the restraint in total cellular output observed *in vitro* (Figures 6D and 6E; Figures S7A–S7E). In contrast, mice repopulated with TFEB$^{H240R\text{-}I243N}$ OE cells showed only modest reductions (Figures 6D and 6E; Figures S7A–S7E). Remarkably, despite their lower repopulation, TFEB^{WT}, but not TFEB$^{H240R\text{-}I243N}$ cells, showed significant enrichment of self-renewing LT-HSCs, as measured in serial xenotransplantation limiting dilution assays (LDAs), with a 6.6-fold increase in stem cell frequency (Figure 6F; Figures S7F and S7G). These results suggest that TFEB governs LT-HSC self-renewal and exerts its effects primarily through DNA binding.

Next we examined the effects of modulating TFEB activity by altering phosphorylation of the S142 site, known to be targeted by several kinases (mTORC1, CDK4/6, and ERK1/2) (Puertollano et al., 2018; Yin et al., 2020). Under nutrient-rich conditions, S142 phosphorylation of TFEB results in its cytoplasmic retention, whereas upon nutrient starvation, dephosphorylated TFEB translocates to the nucleus to induce expression of lysosomal genes (Yin et al., 2020; Napolitano and Ballabio, 2016; Puertollano et al., 2018). OE of a constitutively nuclear form of TFEB (TFEB^{S142A}), generated by disruption of the S142 phosphorylation site, in CD34^{+}CD38^{-} hCB cells led to significant reduction of graft size in primary transplanted mice but a large 22-fold increase in the frequency of self-renewing stem cells (Figures 6D–6F; Figures S6B–S6G and S7A–S7G). The greater enrichment of stem cell frequency in TFEB^{S142} compared with TFEB^{WT} OE cells suggests that regulation of TFEB subcellular localization is important for LT-HSC self-renewal (Figures 6D–6F; Figures S7F and S7G).

Silencing TFEB in CD34^{+}CD38^{-} hCB cells also resulted in a smaller graft size in primary mouse recipients, but in contrast to the findings with TFEB OE vectors, the reduced engraftment in the shTFEB group was now accompanied by a 2.8-fold reduction in stem cell frequency by serial LDA (Figures 6G and 6H; Figures S7H–S7N). Importantly, the *in vitro* reduction in lysosomal numbers observed upon TFEB silencing and the myeloid and erythroid bias induced by TFEB OE and TFEB knockdown, respectively, were recapitulated in xenotransplantation experiments (Figures S7O–S7R). Interestingly, Lyso^{H} LT-HSCs produced fewer GlyA^{+} cells and exhibited a 3.8-fold increase in stem cell frequency despite showing a small reduction in graft size and no differences in LT-HSC abundance in primary transplants compared with Lyso^{L} LT-HSCs, strengthening the link between lysosomal activity and LT-HSC stemness potential (Figures 7A–7E; Figures S7S and S7T). LT-HSC self-renewal requires the TFEB-regulated lysosomal program to limit LT-HSC metabolic activity and expansion, whereas inhibition of this program leads to LT-HSC activation followed by exhaustion.

DISCUSSION

Here we identified an organelle-based model of stem cell fate determination where TFEB and MYC balance the activity of lysosomes to regulate the self-renewal and differentiation properties of human LT-HSCs. In an unperturbed homeostatic setting, TFEB (normally implicated in stress responses) induces constitutive lysosomal flux in LT-HSCs that actively maintains quiescence, preserves self-renewal, and governs lineage commitment. These effects are tied to endolysosomal degradation of membrane receptors, pointing to a role of TFEB in coordinating how LT-HSCs sense environmental changes and initiate the earliest steps of their fate transitions and lineage commitment decisions. Such transitions are delicately balanced by a TFEB/MYC dichotomy where MYC is a driver of LT-HSC anabolism and activation, counteracting TFEB function by serving as a negative transcriptional regulator of lysosomes; conversely, TFEB counteracts MYC activity. TFEB activation is regulated post-transcriptionally through phosphorylation and subcellular localization by upstream kinases and results in limiting LT-HSC quiescence and self-renewal.

Moreover, our study also highlights important discrepancies between mouse and human HSCs. Although nuclear TFEB localization in HSCs has not been reported before, increased TFEB expression has been described in a subset of mouse HSCs with low mitochondrial membrane potential and enhanced quiescence (Liang et al., 2020). However, in contrast to our data, the authors showed that suppression of lysosomal activity by *in vitro* mouse HSC treatment with concanamycin A enhances quiescence and primary engraftment potential (Liang et al., 2020). Future genetic and functional studies specifically targeting the lysosomes and TFEB in mouse HSCs will be required to shed light on these interspecies differences.

Our findings point to a mechanism whereby the TFEB-induced lysosomal program actively maintains LT-HSCs in a quiescent state via endosomal trafficking of external sensing machinery, including signaling and nutrient uptake receptors, to lysosomes for degradation, as exemplified here by the iron transporter TfR1. We hypothesize that this endolysosomal system renders

Please cite this article in press as: García-Prat et al., TFEB-mediated endolysosomal activity controls human hematopoietic stem cell fate, Cell Stem Cell (2021), https://doi.org/10.1016/j.stem.2021.07.003

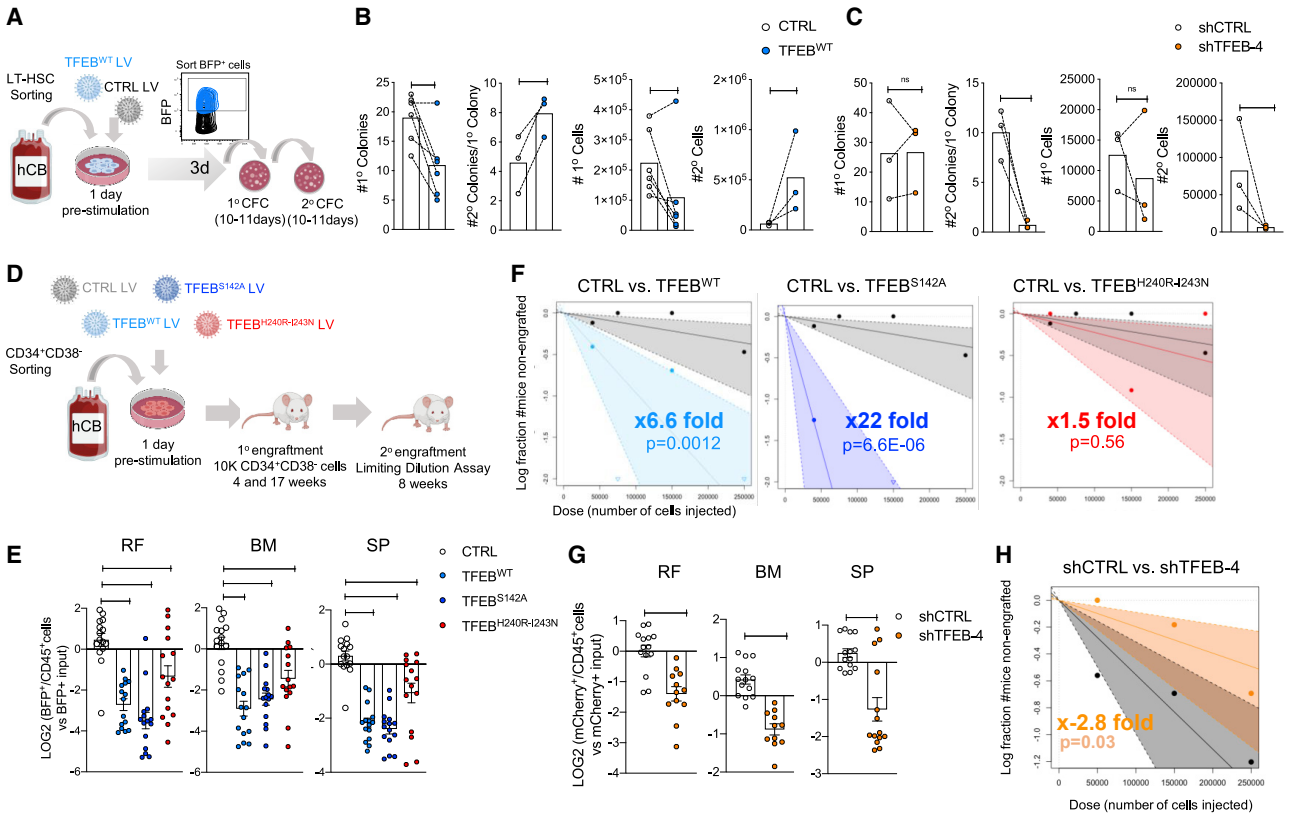

Figure 6. TFEB controls LT-HSC self-renewal

(A) Experimental scheme. LT-HSCs were cultured for 1 day prior to transduction with lentiviral vectors expressing BFP and CTRL or TFEB^{WT}. BFP^{+} cells were sorted at 3 days for serial CFC assays.

(B) Colonies were scored under the microscope, and the number of cells was analyzed by flow cytometry after 10–11 days of plating. 2° and 3° CFC assays were performed following the same protocol and timing. n = 3–6 CB. Paired t test.

(C) Sorted LT-HSCs were cultured for 1 day prior to transduction with lentiviral vectors expressing mCherry and shCTRL or shTFEB. mCherry^{+} cells were sorted at 6 days for serial CFC assays as in (A).

(D) Experimental scheme. CD34^{+}CD38^{-} cells isolated from hCB were transduced with lentiviral vectors expressing BFP and one of the following genes: CTRL, TFEB^{WT}, TFEB^{S142A}, or TFEB$^{H240R\text{-}I243N}$. 1 day after transduction, cells were injected intrafemorally into 8- to 10-week-old NSG-W41 and NSG mice. Male NSG mice were sacrificed 4 weeks and female NSG and male NSG-W41 mice 17 weeks after xenotransplantation for analysis. CD45^{+}/BFP^{+} cells were sorted from primary NSG mice at 17 weeks for secondary limiting dilution assays (LDAs) in NSG-GM3 mice. NSG-GM3 mice were sacrificed 8 weeks after xenotransplantation for stem cell frequency analysis.

(E) From (D): LOG2 ratio of %BFP^{+} in hCD45^{+} cells at 17w of engraftment in NSG-W41 mice versus input (3d post-transduction).

(F) From (D): stem cell frequency calculated from LDA. See Figures S7F and S7G.

(G) As in (D), using an LV expressing mCherry and shCTRL or shTFEB; LOG2 ratio of percent mCherry^{+} in hCD45^{+} cells at 17 weeks of engraftment in NSG-W41 mice versus input (3 days after transduction).

(H) From (G): stem cell frequency calculated from LDA. See Figures S7M and S7N.

Each *in vivo* experiment was performed with three independent CB per experiment with 4–5 mice/CB/condition. RF, right femur, injected bone; BM, left femur and right and left tibiae; SP, spleen. *p < 0.05, **p < 0.01, ***p < 0.001, ****p < 0.0001. Unpaired t test unless otherwise indicated. See also Figure S7.

quiescent LT-HSCs more refractory to specific environmental cues to restrain aberrant mitogenic and anabolic activation and prevent LT-HSC exhaustion, as shown by our TFEB and TfR1 knockdown experiments. Quiescent mouse HSCs express lower membrane levels of TfR1 compared with progenitor cells, which require higher levels of iron uptake for proliferation, and its deletion resulted in profound reconstitution defects (Wang et al., 2019). Regulation of TfR1 by lysosomes in qLT-HSCs may have a protective role by preventing iron overload and the resultant ROS production that would be detrimental to HSC self-renewal (Muto et al., 2017). Our findings regarding TfR1 also help explain an emerging body of work on how lineage determination often occurs already in the stem cell compartment rather than oligopotent progenitors (Notta et al., 2016). Active suppression of TFEB and its downstream lysosomal degradation of TfR1 in LT-HSCs is required for commitment along the erythroid lineage; indeed, activation of TFEB can abolish erythroid differentiation even after lineage commitment has occurred. Our transcriptomics analysis of TFEB^{WT} OE LT-HSCs indicates that endolysosomal degradation of other membrane receptors, such as IGF1R (insulin receptor), which is upstream of the phosphatidylinositol 3-kinase (PI3K)-Akt-mTORC1 pathway, could also be taking place in qLT-HSCs, a finding consistent with observed EGFR degradation in neural stem cells (Kobayashi

Please cite this article in press as: García-Prat et al., TFEB-mediated endolysosomal activity controls human hematopoietic stem cell fate, Cell Stem Cell (2021), https://doi.org/10.1016/j.stem.2021.07.003

CellPress
OPEN ACCESS

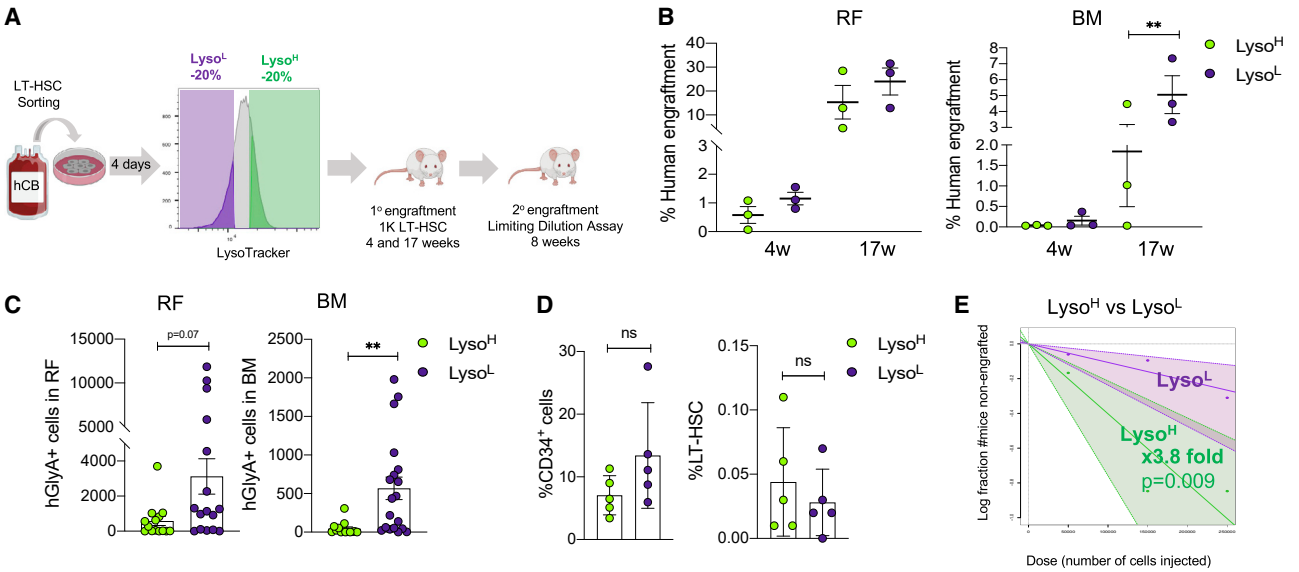

Figure 7. Lysosomal activity governs LT-HSC self-renewal

(A) Experimental scheme: LT-HSCs isolated from hCB were cultured for 4 days and stained with LysoTracker to sort LysoH and LysoL LT-HSCs (1,000 cells/mice) that were injected intrafemorally into 8- to 10-week-old male NSG-W41 mice. NSG-W41 mice were sacrificed 4 and 17 weeks after xenotransplantation for analysis. $CD45^+$ human cells were sorted from primary NSG-W41 mice at 17 weeks for secondary LDAs in NSG-GM3 mice. NSG-GM3 mice were sacrificed 8 weeks after xenotransplantation for stem cell frequency analysis.

(B) From (A): percentage of total $CD45^+$ human cells at 4 and 17 weeks of engraftment in male NSG-W41 mice.

(C) From (A): percentage of $GlyA^+$ from total $hCD45^+$ cells analyzed by flow cytometry at 17 weeks of xenotransplantation in NSG-W41 mice.

(D) From (A): percentage of $CD34^+$ and LT-HSCs at 17 weeks of engraftment in male NSG-W41 mice

(E) From (A): stem cell frequency calculated from LDA. See Figures S7S and S7T.

Each *in vivo* experiment was performed with 3 independent CB pools, and each dot represents an injected mouse (4–5 mice/CB). *$p < 0.05$, **$p < 0.01$, ***$p < 0.001$, ****$p < 0.0001$. Unpaired t test unless otherwise indicated.

et al., 2019). Thus, it is highly likely that the dichotomous TFEB/MYC-mediated control of lysosomal activity will be relevant in other tissue-specific adult stem cells, such as neural and muscle stem cells, that are maintained in quiescence for prolonged periods of time. Our work sheds light on the transcriptional control of lysosomes and its crucial role in stemness regulation, opening new routes to explore in regenerative medicine.

Limitations of the study

In our study, we demonstrate that TFEB and MYC dichotomously regulate the expression of lysosome-associated genes. Because ChiP-seq requires large cell numbers unachievable with rare human LT-HSCs, we relied upon RNA, ATAC-seq, and computational analysis of public data, including cell lines. This required us to look at TFEB binding on mononuclear hCB cells and MYC binding on publicly available ChiP-seq datasets. Moreover, current technical limitations of maintaining the LT-HSC state *in vitro*, required for selection of knockout clones by the CRISPR-Cas9 system, prevents examination of the *TFEB*, *LAMP-1*, or *TFRC* knockout phenotype in human LT-HSCs. Instead, we used shRNA to suppress their expression, achieving 50%–80% reduction in LT-HSCs.

STAR★METHODS

Detailed methods are provided in the online version of this paper and include the following:

- KEY RESOURCES TABLE
- RESOURCE AVAILABILITY
  - Lead contact
  - Materials availability
  - Data and code availability
- EXPERIMENTAL MODEL AND SUBJECT DETAILS
  - Human cord blood samples
  - Mice
- METHOD DETAILS
  - Flow Cytometric Analysis and Sorting
  - Immunostaining analysis
  - Time-lapse imaging
  - Cloning of lentiviral overexpression constructs
  - Cloning of lentiviral knockdown constructs
  - Lentiviral Production and Transduction
  - Cell Culture
  - Colony-Forming Cell Assays
  - Single-Cell Stromal Assays
  - Xenotransplantation
  - Quantitative RT-PCR for TFEB/LAMP1/TFRC knockdown and TFEB overexpression
  - RNA-seq processing and analysis
  - Transcriptomic analysis of published datasets
  - Pathway enrichment analysis and visualization
  - scRNA-seq Signature Enrichment
  - Comparison of TFEB-regulated genes in MEP F2/3 with uncultured CB populations

- ATAC-seq processing and analysis
- Chromatin Immunoprecipitation (ChiP)
- Antibodies used for ChiP
- ChiP-sequencing analysis

- QUANTIFICATION AND STATISTICAL ANALYSIS

SUPPLEMENTAL INFORMATION

Supplemental information can be found online at https://doi.org/10.1016/j.stem.2021.07.003.

ACKNOWLEDGMENTS

We thank the obstetrics units of Trillium Health, William Osler, and Credit Valley Hospitals for CB; the UHN-Sickkids flow cytometry facility for cell sorting; the Advance Optical Microscope Facility (AOMF) for confocal microscopy; Linda Penn, Jason DeMelo, and Aaliya Tamachi for the MYC overexpression vector, and all lab members of the Dick lab for critical feedback. This work was supported by funds to J.E.D. from the Princess Margaret Cancer Centre through funding provided by the Ontario Ministry of Health, Princess Margaret Cancer Centre Foundation, Ontario Institute for Cancer Research through funding provided by the Government of Ontario, Canadian Institutes for Health Research (RN380110-409786), International Development Research Centre Ottawa Canada, Canadian Cancer Society (703212), a Terry Fox New Frontiers Program project grant, University of Toronto's Medicine by Design initiative with funding from the Canada First Research Excellence Fund, and a Canada Research Chair. L.G.-P. was supported by an EMBO long-term fellowship (ALTF 420-2017), a Benjamin Pearl fellowship, and a CIHR fellowship (201910MFE-430959-284655). W.W. was supported by a SystemsX Swiss Initiative in Systems Biology transition postdoctoral fellowship and an ETH career seed grant. T.S. was supported by SNF grant 179490.

AUTHOR CONTRIBUTIONS

L.G.-P. conceived the study, performed research, analyzed data, and wrote the manuscript. F.S. and W.W. performed research and analyzed data. J.C., O.I.G., J.L.M., S.A.S., M.C.S., D.P., K.P., G.K., K.G., S.-I.T., and E.W. performed research. V.V., A.M., A.G.X.Z., and M.C.-S.-Y. analyzed data. K.B.K. and S.Z.X. performed research and wrote the manuscript. M.L. and T.S. supervised research and secured funding. J.E.D. wrote the manuscript, secured funding, and supervised the study.

DECLARATION OF INTERESTS

J.E.D. received research funding from Celgene and serves on the Advisory Board of Trillium Therapeutics.

Received: April 22, 2021
Revised: June 15, 2021
Accepted: June 23, 2021
Published: August 2, 2021

REFERENCES

Anders, S., Pyl, P.T., and Huber, W. (2015). HTSeq–a Python framework to work with high-throughput sequencing data. Bioinformatics *31*, 166–169.

Annunziata, I., van de Vlekkert, D., Wolf, E., Finkelstein, D., Neale, G., Machado, E., Mosca, R., Campos, Y., Tillman, H., Roussel, M.F., et al. (2019). MYC competes with MiT/TFE in regulating lysosomal biogenesis and autophagy through an epigenetic rheostat. Nat. Commun. *10*, 3623.

Buenrostro, J.D., Giresi, P.G., Zaba, L.C., Chang, H.Y., and Greenleaf, W.J. (2013). Transposition of native chromatin for fast and sensitive epigenomic profiling of open chromatin, DNA-binding proteins and nucleosome position. Nat. Methods *10*, 1213–1218.

Cabezas-Wallscheid, N., Buettner, F., Sommerkamp, P., Klimmeck, D., Ladel, L., Thalheimer, F.B., Pastor-Flores, D., Roma, L.P., Renders, S., Zeisberger, P., et al. (2017). Vitamin A-Retinoic Acid Signaling Regulates Hematopoietic Stem Cell Dormancy. Cell *169*, 807–823.e19.

Cao, H., Schroeder, B., Chen, J., Schott, M.B., and McNiven, M.A. (2016). The Endocytic Fate of the Transferrin Receptor Is Regulated by c-Abl Kinase. J. Biol. Chem. *291*, 16424–16437.

Dobin, A., Davis, C.A., Schlesinger, F., Drenkow, J., Zaleski, C., Jha, S., Batut, P., Chaisson, M., and Gingeras, T.R. (2013). STAR: ultrafast universal RNA-seq aligner. Bioinformatics *29*, 15–21.

ENCODE Project Consortium (2012). An integrated encyclopedia of DNA elements in the human genome. Nature *489*, 57–74.

García-Prat, L., Martínez-Vicente, M., Perdiguero, E., Ortet, L., Rodríguez-Ubreva, J., Rebollo, E., Ruiz-Bonilla, V., Gutarra, S., Ballestar, E., Serrano, A.L., et al. (2016). Autophagy maintains stemness by preventing senescence. Nature *529*, 37–42.

García-Prat, L., Sousa-Victor, P., and Muñoz-Cánoves, P. (2017). Proteostatic and Metabolic Control of Stemness. Cell Stem Cell *20*, 593–608.

Ghaffari, S. (2021). Lysosomal Regulation of Metabolism in Quiescent Hematopoietic Stem Cells: More than Just Autophagy. Cell Stem Cell *28*, 374–377.

Heinz, S., Benner, C., Spann, N., Bertolino, E., Lin, Y.C., Laslo, P., Cheng, J.X., Murre, C., Singh, H., and Glass, C.K. (2010). Simple combinations of lineage-determining transcription factors prime cis-regulatory elements required for macrophage and B cell identities. Mol. Cell *38*, 576–589.

Hilsenbeck, O., Schwarzfischer, M., Skylaki, S., Schauberger, B., Hoppe, P.S., Loeffler, D., Kokkaliaris, K.D., Hastreiter, S., Skylaki, E., Filipczyk, A., et al. (2016). Software tools for single-cell tracking and quantification of cellular and molecular properties. Nat. Biotechnol. *34*, 703–706.

Hilsenbeck, O., Schwarzfischer, M., Loeffler, D., Dimopoulos, S., Hastreiter, S., Marr, C., Theis, F.J., and Schroeder, T. (2017). fastER: a user-friendly tool for ultrafast and robust cell segmentation in large-scale microscopy. Bioinformatics *33*, 2020–2028.

Ho, T.T., Warr, M.R., Adelman, E.R., Lansinger, O.M., Flach, J., Verovskaya, E.V., Figueroa, M.E., and Passegué, E. (2017). Autophagy maintains the metabolism and function of young and old stem cells. Nature *543*, 205–210.

Hu, Y., and Smyth, G.K. (2009). ELDA: extreme limiting dilution analysis for comparing depleted and enriched populations in stem cell and other assays. J. Immunol. Methods *347*, 70–78.

Ito, K., Turcotte, R., Cui, J., Zimmerman, S.E., Pinho, S., Mizoguchi, T., Arai, F., Runnels, J.M., Alt, C., Teruya-Feldstein, J., et al. (2016). Self-renewal of a purified Tie2+ hematopoietic stem cell population relies on mitochondrial clearance. Science *354*, 1156–1160.

Ito, K., Bonora, M., and Ito, K. (2019). Metabolism as master of hematopoietic stem cell fate. Int. J. Hematol. *109*, 18–27.

Itoh, K., Tezuka, H., Sakoda, H., Konno, M., Nagata, K., Uchiyama, T., Uchino, H., and Mori, K.J. (1989). Reproducible establishment of hemopoietic supportive stromal cell lines from murine bone marrow. Exp. Hematol. *17*, 145–153.

Kaufmann, K.B., Garcia-Prat, L., Liu, Q., Ng, S.W.K., Takayanagi, S.I., Mitchell, A., Wienholds, E., van Galen, P., Cumbaa, C.A., Tsay, M.J., et al. (2019). A stemness screen reveals *C3orf54/INKA1* as a promoter of human leukemia stem cell latency. Blood *133*, 2198–2211.

Knott, S.R.V., Maceli, A., Erard, N., Chang, K., Marran, K., Zhou, X., Gordon, A., Demerdash, O.E., Wagenblast, E., Kim, S., et al. (2014). A computational algorithm to predict shRNA potency. Mol. Cell *56*, 796–807.

Kobayashi, T., Piao, W., Takamura, T., Kori, H., Miyachi, H., Kitano, S., Iwamoto, Y., Yamada, M., Imayoshi, I., Shioda, S., et al. (2019). Enhanced lysosomal degradation maintains the quiescent state of neural stem cells. Nat. Commun. *10*, 5446.

Laurenti, E., and Göttgens, B. (2018). From haematopoietic stem cells to complex differentiation landscapes. Nature *553*, 418–426.

Laurenti, E., Varnum-Finney, B., Wilson, A., Ferrero, I., Blanco-Bose, W.E., Ehninger, A., Knoepfler, P.S., Cheng, P.F., MacDonald, H.R., Eisenman, R.N., et al. (2008). Hematopoietic stem cell function and survival depend on c-Myc and N-Myc activity. Cell Stem Cell *3*, 611–624.

Laurenti, E., Doulatov, S., Zandi, S., Plumb, I., Chen, J., April, C., Fan, J.B., and Dick, J.E. (2013). The transcriptional architecture of early human hematopoiesis identifies multilevel control of lymphoid commitment. Nat. Immunol. *14*, 756–763.

Laurenti, E., Frelin, C., Xie, S., Ferrari, R., Dunant, C.F., Zandi, S., Neumann, A., Plumb, I., Doulatov, S., Chen, J., et al. (2015). CDK6 levels regulate quiescence exit in human hematopoietic stem cells. Cell Stem Cell *16*, 302–313.

Lawrence, R.E., and Zoncu, R. (2019). The lysosome as a cellular centre for signalling, metabolism and quality control. Nat. Cell Biol. *21*, 133–142.

Leeman, D.S., Hebestreit, K., Ruetz, T., Webb, A.E., McKay, A., Pollina, E.A., Dulken, B.W., Zhao, X., Yeo, R.W., Ho, T.T., et al. (2018). Lysosome activation clears aggregates and enhances quiescent neural stem cell activation during aging. Science *359*, 1277–1283.

Li, H., and Durbin, R. (2009). Fast and accurate short read alignment with Burrows-Wheeler transform. Bioinformatics *25*, 1754–1760.

Liang, R., Arif, T., Kalmykova, S., Kasianov, A., Lin, M., Menon, V., Qiu, J., Bernitz, J.M., Moore, K., Lin, F., et al. (2020). Restraining Lysosomal Activity Preserves Hematopoietic Stem Cell Quiescence and Potency. Cell Stem Cell *26*, 359–376.e7.

Loeffler, D., Wehling, A., Schneiter, F., Zhang, Y., Müller-Bötticher, N., Hoppe, P.S., Hilsenbeck, O., Kokkaliaris, K.D., Endele, M., and Schroeder, T. (2019). Asymmetric lysosome inheritance predicts activation of haematopoietic stem cells. Nature *573*, 426–429.

Luzio, J.P., Hackmann, Y., Dieckmann, N.M., and Griffiths, G.M. (2014). The biogenesis of lysosomes and lysosome-related organelles. Cold Spring Harb. Perspect. Biol. *6*, a016840.

Martina, J.A., Diab, H.I., Li, H., and Puertollano, R. (2014). Novel roles for the MiTF/TFE family of transcription factors in organelle biogenesis, nutrient sensing, and energy homeostasis. Cell. Mol. Life Sci. *71*, 2483–2497.

Mazurier, F., Doedens, M., Gan, O.I., and Dick, J.E. (2003). Rapid myeloerythroid repopulation after intrafemoral transplantation of NOD-SCID mice reveals a new class of human stem cells. Nat. Med. *9*, 959–963.

Moura, I.C., Hermine, O., Lacombe, C., and Mayeux, P. (2015). Erythropoiesis and transferrin receptors. Curr. Opin. Hematol. *22*, 193–198.

Muto, Y., Nishiyama, M., Nita, A., Moroishi, T., and Nakayama, K.I. (2017). Essential role of FBXL5-mediated cellular iron homeostasis in maintenance of hematopoietic stem cells. Nat. Commun. *8*, 16114.

Mutvei, A.P., Nagiec, M.J., Hamann, J.C., Kim, S.G., Vincent, C.T., and Blenis, J. (2020). Rap1-GTPases control mTORC1 activity by coordinating lysosome organization with amino acid availability. Nat. Commun. *11*, 1416.

Napolitano, G., and Ballabio, A. (2016). TFEB at a glance. J. Cell Sci. *129*, 2475–2481.

Notta, F., Zandi, S., Takayama, N., Dobson, S., Gan, O.I., Wilson, G., Kaufmann, K.B., McLeod, J., Laurenti, E., Dunant, C.F., et al. (2016). Distinct routes of lineage development reshape the human blood hierarchy across ontogeny. Science *351*, aab2116.

Palm, W., and Thompson, C.B. (2017). Nutrient acquisition strategies of mammalian cells. Nature *546*, 234–242.

Palmieri, M., Impey, S., Kang, H., di Ronza, A., Pelz, C., Sardiello, M., and Ballabio, A. (2011). Characterization of the CLEAR network reveals an integrated control of cellular clearance pathways. Hum. Mol. Genet. *20*, 3852–3866.

Pellin, D., Loperfido, M., Baricordi, C., Wolock, S.L., Montepeloso, A., Weinberg, O.K., Biffi, A., Klein, A.M., and Biasco, L. (2019). A comprehensive single cell transcriptional landscape of human hematopoietic progenitors. Nat. Commun. *10*, 2395.

Puertollano, R., Ferguson, S.M., Brugarolas, J., and Ballabio, A. (2018). The complex relationship between TFEB transcription factor phosphorylation and subcellular localization. EMBO J. *37*, e98804.

Reimand, J., Isserlin, R., Voisin, V., Kucera, M., Tannus-Lopes, C., Rostamianfar, A., Wadi, L., Meyer, M., Wong, J., Xu, C., et al. (2019). Pathway enrichment analysis and visualization of omics data using g:Profiler, GSEA, Cytoscape and EnrichmentMap. Nat. Protoc. *14*, 482–517.

Subramanian, A., Tamayo, P., Mootha, V.K., Mukherjee, S., Ebert, B.L., Gillette, M.A., Paulovich, A., Pomeroy, S.L., Golub, T.R., Lander, E.S., and Mesirov, J.P. (2005). Gene set enrichment analysis: A knowledge-based approach for interpreting genome-wide expression profiles. PNAS *102*, 15545–15550.

van Galen, P., Hovestadt, V., Wadsworth Ii, M.H., Hughes, T.K., Griffin, G.K., Battaglia, S., Verga, J.A., Stephansky, J., Pastika, T.J., Lombardi Story, J., et al. (2019). Single-Cell RNA-Seq Reveals AML Hierarchies Relevant to Disease Progression and Immunity. Cell *176*, 1265–1281.e24.

Velten, L., Haas, S.F., Raffel, S., Blaszkiewicz, S., Islam, S., Hennig, B.P., Hirche, C., Lutz, C., Buss, E.C., Nowak, D., et al. (2017). Human haematopoietic stem cell lineage commitment is a continuous process. Nat. Cell Biol. *19*, 271–281.

Wagenblast, E., Azkanaz, M., Smith, S.A., Shakib, L., McLeod, J.L., Krivdova, G., Araújo, J., Shultz, L.D., Gan, O.I., Dick, J.E., and Lechman, E.R. (2019). Functional profiling of single CRISPR/Cas9-edited human long-term hematopoietic stem cells. Nat. Commun. *10*, 4730.

Wang, S., He, X., Wu, Q., Jiang, L., Chen, L., Yu, Y., Zhang, P., Huang, X., Wang, J., Ju, Z., et al. (2019). Transferrin receptor 1-mediated iron uptake plays an essential role in hematopoiesis. Haematologica.

Wilson, A., Murphy, M.J., Oskarsson, T., Kaloulis, K., Bettess, M.D., Oser, G.M., Pasche, A.C., Knabenhans, C., Macdonald, H.R., and Trumpp, A. (2004). c-Myc controls the balance between hematopoietic stem cell self-renewal and differentiation. Genes Dev. *18*, 2747–2763.

Xie, S.Z., Garcia-Prat, L., Voisin, V., Ferrari, R., Gan, O.I., Wagenblast, E., Kaufmann, K.B., Zeng, A.G.X., Takayanagi, S.I., Patel, I., et al. (2019). Sphingolipid Modulation Activates Proteostasis Programs to Govern Human Hematopoietic Stem Cell Self-Renewal. Cell Stem Cell *25*, 639–653.e7.

Yin, Q., Jian, Y., Xu, M., Huang, X., Wang, N., Liu, Z., Li, Q., Li, J., Zhou, H., Xu, L., et al. (2020). CDK4/6 regulate lysosome biogenesis through TFEB/TFE3. J. Cell Biol. *219*, e201911036.

Zhang, Y., Liu, T., Meyer, C.A., Eeckhoute, J., Johnson, D.S., Bernstein, B.E., Nusbaum, C., Myers, R.M., Brown, M., Li, W., and Liu, X.S. (2008). Model-based analysis of ChIP-Seq (MACS). Genome Biol. *9*, R137.

Please cite this article in press as: García-Prat et al., TFEB-mediated endolysosomal activity controls human hematopoietic stem cell fate, Cell Stem Cell (2021), https://doi.org/10.1016/j.stem.2021.07.003

STAR★METHODS

KEY RESOURCES TABLE

REAGENT or RESOURCE	SOURCE	IDENTIFIER
Antibodies		
FITC–anti-CD45 (2D1)	BD	Cat#347463; RRID:AB_400306
PE–anti-CD90 (5E10)	BD	Cat#555596; RRID:AB_395970
PECy5–anti-CD49f (GoH3)	BD	Cat#551129; RRID:AB_394062
V450–anti-CD7 (M-T701)	BD	Cat# 642916; RRID:AB_1645757
PECy7–anti-CD38 (HB7)	BD	Cat#335790; RRID:AB_399969
APC–anti-CD10 (HI10a)	BD	Cat# 340923; RRID:AB_400543
APCCy7–anti-CD34 (581)	BD	custom made by BD
BV711-anti-CD19 (SJ25C1)	BD	Cat#563036; RRID:AB_2737968
Alexafluor700–anti-CD7 (M-T701)	BD	Cat# 561603; RRID:AB_10898348
V500-anti-CD45 (HI30)	BD	Cat#560777; RRID:AB_1937324
biotin-Flt3L	BD	N/A
Streptavidin-Qdot605	ThermoFisher	Cat#Q10101MP
Streptavidin-PE	BD	Cat# 554061; RRID:AB_10053328
V450-anti-CD15 (MMA)	BD	Cat# 642917; RRID:AB_1645751
FITC-anti-CD3 (SK7)	BD	Cat#349201; RRID:AB_400405
PE–anti-CD19 (4G7)	BD	Cat#349209; RRID:AB_400407
PE–anti-GlyA (11E4B-7-6)	Beckman Coulter	Cat#A07792
BV786–anti-CD33 (WM53)	BD	Cat#740974; RRID:AB_2740599
PECy5–anti-CD45 (J33)	Beckman Coulter	Cat#A07785
PECy7–anti-CD14 (RMO52)	Beckman Coulter	Cat# A22331; RRID:AB_10639528
APC–anti-CD33 (WM53)	BD	Cat# 551378; RRID:AB_398502
APC–anti-CD45 (2D1)	BD	Cat#340943; RRID:AB_400555
V421–anti-CD10 (HI10a)	BD	Cat# 562902; RRID:AB_2737879
BV605-anti-CD56 (NCAM16.2)	BD	Cat#562780; RRID:AB_2728700
PE-anti-CD71 (M-A712)	BD	Cat# 555537; RRID:AB_395921
APCCy7-anti-CD41 (P2)	Beckman Coulter	Cat#6607115;RRID:AB_2800448
BV786-anti-CD71 (M-A712)	BD	Cat# 563768; RRID:AB_2738414
PE-anti-Ki67 (B56)	BD	Cat#556027; RRID:AB_2266296
Anti-TFEB	R&D biosystems	Cat#MAB9170-100
Anti- MYC Alexa647	R&D biosystems	Cat#IC36961R-100ug
Anti-LAMP1 Alexa488	R&D biosystems	Cat#IC7985G
Anti-CD71 APC (M-A712)	BD	Cat# 551374; RRID:AB_398500
Purified Mouse Anti-Human CD71 (M-A712)	BD	Cat# 555534; RRID:AB_395918
Human Cathepsin D Antibody	R&D biosystems	Cat# AF1014; RRID:AB_2087218
Goat Anti-mouse secondary antibody Alexa568	Thermo Fisher	Cat#A-11004; RRID:AB_2534072
Goat Anti-rabbit secondary antibody Alexa488	Thermo Fisher	Cat# A-11008; RRID:AB_143165
Normal Rabbit IgG antibody	Cell Signaling Technology	Cat# 2729; RRID:AB_1031062
Histone H3 (acetyl K27) antibody	Abcam	Cat# ab4729; RRID:AB_2118291
TFEB antibody (ChiP-seq)	Cell Signaling Technology	Cat# 4240S
TFEB antibody (ChiP-seq)	Cell Signaling Technology	Cat# D2O7D
TFEB (C-6) antibody (ChiP-seq)	Santa Cruz Biotechnology	Cat# sc-166736; RRID:AB_2255943
Biological samples		
Human umbilical cord blood samples	Trillium, Credit Valley and Brampton Civic Hospital	N/A

(*Continued on next page*)

Please cite this article in press as: García-Prat et al., TFEB-mediated endolysosomal activity controls human hematopoietic stem cell fate, Cell Stem Cell (2021), https://doi.org/10.1016/j.stem.2021.07.003

Continued

REAGENT or RESOURCE	SOURCE	IDENTIFIER
Chemicals, peptides, and recombinant proteins		
DNase I	Roche	Cat#11284932001
Ammonium Chloride	Stem Cell Technologies	Cat#07850
FLT3 Ligand	Milteny Biotec	Cat#130-096-480
IL6	Milteny Biotec	Cat#130-093-934
SCF	Milteny Biotec	Cat#130-096-696
TPO	Milteny Biotec	Cat#130-095-752
EPO	Janssen	Eprex 10,000 IU/ml
IL3	Milteny Biotec	Cat#130-095-068
GM-CSF	Milteny Biotec	Cat#130-093-866
AmpliTaq Gold 360 Polymerase	ThermoFisher	Cat#4398813
BamH1-HF	NEB	Cat#R0136S
Mlu1-HF	Invitrogene	Cat#15432-016
KOD Hot Start DNA Polymerase	Millipore-Sigma	Cat#71842
DpnI	New England Biolabs	Cat#R0176S
Paraformaldehyde 16% Solution (methanol-free)	Agar scientific	Cat#AGR1026
Poly-L-lysine solution	Sigma	Cat#P8920
IGEPAL® CA-630	Sigma	Cat#I8896-50ML
DMSO	Fisher Chemical	Cat#D128-500
Bafilomycin A1	Sigma	Cat#B1793
MYC inhibitor	Milipore-sigma	Cat#475956-10MG
DAPI	Sigma	Cat#10236276001
Fluoromount G	Thermo Fisher	Cat#00-4958-02
Tween 20	Sigma	Cat#P9416-100ML
Triton X-100	Sigma	Cat#T8787-100
Critical commercial assays		
StemSep Human Hematopoietic Progenitor Cell Enrichment Kit	Stem Cell Technologies	Cat#14066
CD34 MicroBead Kit, human	Milteny Biotec	Cat#130-097-047
LS Columns	Milteny Biotec	Cat#130-042-401
Mouse Cell Depletion Kit	Milteny Biotec	Cat#130-104-694
SuperScript VILO	ThermoFisher	Cat#1754050
Power SYBR Green	ThermoFisher	Cat#4367659
Magic Red Cathepsin B Kit	BioRad	Cat#ICT937
RNeasy Micro Kit	QIAGEN	Cat#74004
PicoPure® RNA Isolation Kit	Thermo Fisher	Cat#KIT0204
Gateway™ LR Clonase™ II Enzyme Mix	Thermo Fisher	Cat#11791020
CYTO-ID® Autophagy detection kit	Enzo Life Sciences	Cat#ENZ-51031-K200
RNase-Free DNase Set (50)	QIAGEN	Cat#79254
Click-iT® Plus EdU Alexa Fluor® 647 Flow Cytometry	Thermo Fisher	Cat#C10634
CellROX Deep Red	ThermoFisher	Cat#C10422
CellROX Orange	ThermoFisher	Cat#C10443
MitoTracker Green	ThermoFisher	Cat#M7514
LysoTracker Blue	ThermoFisher	Cat#L7525
LysoTracker Green	ThermoFisher	Cat#L7526
LysoTracker Deep Red	ThermoFisher	Cat#L12492
LysoSensor Green DND-189	ThermoFisher	Cat#L7535
RNeasy Plus Micro Kit	QIAGEN	Cat#74034

(*Continued on next page*)

Please cite this article in press as: García-Prat et al., TFEB-mediated endolysosomal activity controls human hematopoietic stem cell fate, Cell Stem Cell (2021), https://doi.org/10.1016/j.stem.2021.07.003

Continued

REAGENT or RESOURCE	SOURCE	IDENTIFIER
Sytoxblue	ThermoFisher	Cat#S11348
Propidium Iodide	ThermoFisher	Cat#P3566
BD cytofix/cytoperm fixation solution	BD	Cat#554722
BD PermWash	BD	Cat#554723
Phusion High fildelity PCR master Mix with HF buffer	NEB	Cat#M0531S
MiniElute PCR purification Kit	QIAGEN	Cat#28004
Nextera DNA library prep kit 96 samples	Illumina	Cat#15028211
Syber Green	ThermoFisher	Cat#S7563
Hoechst 33342	Thermo Fisher	Cat#H3570
Monarch PCR & DNA Cleanup kit	New England Biolabs	Cat#T1030L
SensiFast SYBR No-ROX kit	FroggaBio	Cat#BIO 76005
Protease Inhibitor	Roche	Cat#11697498001
Dynabeads Protein A Immunoprecipitation kit	Invitrogene	Cat#10006D
Dynabeads Protein G Immunoprecipitation kit	Invitrogene	Cat#10007D
ThruPLEX DNA-seq kit	Takara Bio	Cat#R400674
Deposited data		
Processed Data Super Series	This manuscript	GEO: GSE153917
$TFEB^{WT}$ versus CTRL LT-HSC ATAC-seq	This manuscript	GEO: GSE153910
MYC^{WT} versus CTRL LT-HSC RNA-seq	This manuscript	GEO: GSE153911
shTFEB versus shCTRL LT-HSC RNA-seq	This manuscript	GEO: GSE153912
$TFEB^{WT}$ versus CTRL LT-HSC RNA-seq	This manuscript	GEO: GSE153913
$TFEB^{WT}$ versus CTRL MEP RNA-seq	This manuscript	GEO: GSE153914
$TFEB^{WT}$ versus CTRL ST-HSC RNA-seq	This manuscript	GEO: GSE153915
Illumina HumanHT-12 beadchip expression data from lineage-depleted human CB cells	Laurenti et al., 2013	GEO: GSE42414
RNA-seq from cell subpopulations isolated from human CB cells	This manuscript and Xie et al., 2019	GEO: GSE125345
single cell RNA-seq data of HSPCs from human bone marrow	Velten et al., 2017	GEO: GSE75478
single cell RNA-seq data of HSPCs from human bone marrow	Pellin et al., 2019	GEO: GSE117498
single cell RNA-seq data of HSPCs from human bone marrow	van Galen et al., 2019	GEO: GSE116256
Raw Data	This manuscript	EGA: EGAD00001006884
Pathway Database	The Bader Lab	http://baderlab.org/GeneSets
Experimental models: Cell lines		
Nalm-6	DSMZ	Cat# ACC-128, RRID:CVCL_0092
MS-5 (murine stroma cell line)	Itoh et al., 1989	N/A
Experimental models: Organisms/strains		
NOD.Cg-PrkdcscidIl2rgtm1Wjl/SzJ (NSG) mice	The Jackson Laboratory	Cat#005557; RRID:IMSR_JAX:005557
NOD.Cg-PrkdcscidIl2rgtm1WjlTg(CMV-IL3,CSF2,KITLG)1Eav/MloySzJ (NSG-SGM3)	The Jackson Laboratory	Cat#013062; RRID:IMSR_JAX:013062
NOD.Cg-PrkdcscidIl2rgtm1WjlKitem1Mvw/SzJ (NSGW41)	The Jackson Laboratory	Cat#026497
Recombinant DNA		
CTRL (gp91_P415H)	Kaufmann et al., 2019	pLBC2-BS lentiviral vector
$TFEB^{WT}$	This manuscript	pLBC2-BS lentiviral vector
$TFEB^{S142A}$	This manuscript	pLBC2-BS lentiviral vector
$TFEB^{H240R\_\ I243N}$	This manuscript	pLBC2-BS lentiviral vector

(*Continued on next page*)

Please cite this article in press as: García-Prat et al., TFEB-mediated endolysosomal activity controls human hematopoietic stem cell fate, Cell Stem Cell (2021), https://doi.org/10.1016/j.stem.2021.07.003

Continued

REAGENT or RESOURCE	SOURCE	IDENTIFIER
shRenilla (shCTRL)	Kaufmann et al., 2019	pLBC2-BS lentiviral vector
shTFEB-4	This manuscript	pLBC2-BS lentiviral vector
shLAMP1	This manuscript	pLBC2-BS lentiviral vector
shTfR1	This manuscript	pLBC2-BS lentiviral vector
Oligonucleotides		
shRenilla sequence: TGCTGTTGACA GTGAGCGCAGGAATTATAATGCTTA TCTATAGTGAAGCCACAGATGTATA GATAAGCATTATAATTCCTATGCCTA CTGCCTCGGA	Kaufmann et al., 2019	N/A
shTFEB-2 sequence: TGCTGTTGAC AGTGAGCGAACGATGTCCTTGGCT ACATCATAGTGAAGCCACAGATGT ATGATGTAGCCAAGGACATCGTCT GCCTACTGCCTCGGA	This manuscript	N/A
shTFEB-3 sequence: TGCTGTTGAC AGTGAGCGAGATGATGTCATTGAC AACATATAGTGAAGCCACAGATGT ATATGTTGTCAATGACATCATCCTG CCTACTGCCTCGGA	This manuscript	N/A
shTFEB-4 sequence: TGCTGTTGA CAGTGAGCGCAGAAAGACAATCA CAACTTAATAGTGAAGCCACAGAT GTATTAAGTTGTGATTGTCTTTCT TTGCCTACTGCCTCGGA	This manuscript	N/A
shTfR1 sequence: TGCTGTTGAC AGTGAGCGCCAGCCAACTGCTTT CATTTGATAGTGAAGCCACAGAT GTATCAAATGAAAGCAGTTGGC TGTTGCCTACTGCCTCGGA	This manuscript	N/A
shLAMP1 sequence: TGCTGTTGA CAGTGAGCGATGGACGAGAACA GCATGCTGATAGTGAAGCCACAG ATGTATCAGCATGCTGTTCTCGT CCAGTGCCTACTGCCTCGGA	This manuscript	N/A
pENTR223-TFEB-S142A fw primer: 5′- CAC CCA TGG CCA TGC TGC AC-3′	This manuscript	N/A
pENTR223-TFEB-S142A rev primer: 5′- CAT TGG GAG CAC TGT TGC CAG C-3′	This manuscript	N/A
pENTR223-TFEB- H240R_ I243N fw primer: 5′- CGG AAC TTA AAT GAA AGG AGA CGA AGG-3′	This manuscript	N/A
pENTR223-TFEB- H240R_ I243N rev primer: 5′- ATT GTC TTT CTT CTG CCG CTC C-3′	This manuscript	N/A
Software and algorithms		
ImageJ/Fiji	ImageJ	https://imagej.net/Downloads
FACSDiva v. 8.0.1.1	BD	N/A
FlowJo10	Flowjo, LLC	https://www.flowjo.com/solutions/flowjo/downloads
STAR v2.5.2b	Dobin et al., 2013	https://github.com/alexdobin/STAR
HTSeq v0.7.2	Anders et al., 2015	https://github.com/simon-anders/htseq
Sherwood algorithm	Knott et al., 2014	N/A
GSEA_4.0.3	(Subramanian et al., 2005)	https://www.gsea-msigdb.org/gsea/index.jsp

(*Continued on next page*)

Please cite this article in press as: García-Prat et al., TFEB-mediated endolysosomal activity controls human hematopoietic stem cell fate, Cell Stem Cell (2021), https://doi.org/10.1016/j.stem.2021.07.003

Continued

REAGENT or RESOURCE	SOURCE	IDENTIFIER
EnrichmentMap version 3.1.0	N/A	https://apps.cytoscape.org/apps/enrichmentmap
Cytoscape 3.7.0	N/A	https://github.com/cytoscape/cytoscape.wiki
g:profiler	N/A	https://biit.cs.ut.ee/gprofiler/gost
BWA (0.7.15)	Li and Durbin, 2009	N/A
MACS (2.2.5)	Zhang et al., 2008	https://github.com/macs3-project/MACS
Homer (4.11.1)	Heinz et al., 2010	N/A
Extreme Limiting Dilution Analysis (ELDA)	Hu and Smyth, 2009	http://bioinf.wehi.edu.au/software/elda/
Prism 8	Graphpad Software	https://www.graphpad.com/scientific-software/prism/
LSM Zen 2012	Zeiss	N/A
Other		
X-vivo medium	Lonza	Cat#04-380Q
H5100 media	StemCell Technologies	Cat#05150
Fetal bovine serum	Sigma	Cat#F1051-500mL
Iscove's modified Dulbecco's medium (IMDM)	GIBCO	Cat#12440-053
MethoCult™Optimum	Stem Cell Technologies	Cat#H4034
StemPro™-34 SFM	GIBCO	Cat#10640-019
StemPro nutrients	GIBCO	Cat#10641-025
L-glutamine	Multicell	Cat#609-065-EL
Pen/Strep	GIBCO	Cat#15140-122
Human LDL	Stem Cell Technologies	Cat#02698
8 Well Chamber, removable	ibidi	Cat#80841
12 Well Chamber, removable	ibidi	Cat#81201

RESOURCE AVAILABILITY

Lead contact

Further information and requests for resources and reagents should be directed to and are available from the lead contact, John E. Dick (john.dick@uhnresearch.ca).

Materials availability

Plasmids generated in this study are available upon request from the lead contact, John E. Dick (john.dick@uhnresearch.ca), but a completed Materials Transfer Agreement may be required.

Data and code availability

- RNA-seq and ATAC-seq processed data has been submitted to the GEO archive (SuperSeries: GSE153917) and raw data at EGA (EGAD00001006884).
- For each analysis performed, the software and version used has been detailed in the STAR Methods section.
- Any additional information required to reanalyze the data reported in this paper is available from the lead contact, John E. Dick (john.dick@uhnresearch.ca) upon request.

EXPERIMENTAL MODEL AND SUBJECT DETAILS

Human cord blood samples

Human CB samples were obtained with informed consent from Trillium Health, Credit Valley and William Osler Hospitals according to procedures approved by the University Health Network (UHN) Research Ethics Board. Mononuclear cells (MNC) from pools of male and female CB units (~4-15 units) were obtained by centrifugation on Lymphoprep medium, and after ammonium chloride lysis MNC were enriched for $CD34^+$ cells by positive selection with the CD34 Microbead kit and LS column purification with MACS magnet technology (Miltenyi). Resulting $CD34^+$ CB cells were viably stored in 50% PBS, 40% fetal bovine serum (FBS) and 10% DMSO at $-80^\circ C$ or $-150^\circ C$.

Please cite this article in press as: García-Prat et al., TFEB-mediated endolysosomal activity controls human hematopoietic stem cell fate, Cell Stem Cell (2021), https://doi.org/10.1016/j.stem.2021.07.003

Mice

Animal experiments were done in accordance with institutional guidelines approved by University Health Network Animal care committee. All *in vivo* experiments were done with 8- to 12-week-old female/male *NOD.Cg-Prkdcscidll2rgtm1Wjl/SzJ* (NSG) mice (JAX) and 8- to 12-week-old female/male *NOD.Cg-Prkdcscidll2rgtm1WjlTg(CMV-IL3,CSF2,KITLG)1Eav/MloySzJ* (NSG-SGM3) that were sublethally irradiated with 225 cGy, 24 h before transplantation, or with 8- to 12-week-old male *NOD.Cg-Prkdcscidll2rgtm1WjlKitem1Mvw/SzJ* (NSGW41) mice that were not irradiated. All mice were housed at the animal facility (ARC) at Princess Margaret Cancer Centre in a room designated only for immunocompromised mice with individually ventilated racks equipped with complete sterile micro-isolator caging (IVC), on corn-cob bedding and supplied with environmental enrichment in the form of a red house/tube and a cotton nestlet. Cages are changed every < 7 days under a biological safety cabinet. Health status is monitored using a combination of soiled bedding sentinels and environmental monitoring.

METHOD DETAILS

Flow Cytometric Analysis and Sorting

Sorting: $CD34^+$ and $CD34^-$ human CB cells were thawed via slow dropwise addition of X-VIVO 10 medium with 50% FBS and DNaseI (200 μg/ml). Cells were spun at 350 g for 10min at 4°C and then resuspended in PBS+2.5% FBS. For all *in vitro* and *in vivo* experiments, the full stem and progenitor hierarchy sort was performed as described in Notta et al. (2016) and shown in Figures S1A and S7B. Cells were resuspended in 100 μL per $1x10^6$ cells and stained in two subsequent rounds for 15 min at room temperature each. See Table 1 for antibodies.

Cell cycle: Cells were cultured with EdU for 1 hour and harvested for EdU Click-it reaction following manufacturer's instructions. Cells were then incubated with PE-anti-Ki67 antibody in PermWash solution overnight at 4°C. Prior to flow cytometry analysis cells were stained with Hoechst 33342.

Cell dyes: Cells were incubated for 30 min at 37°C with the indicated dyes following manufacturer's instructions (CellROX, 5 μM; MitoTracker, 0.1 μM; LysoTracker, 75nM; Magic Red, 1/260 dilution; CytoID, 1/500 dilution; LysoSensor, 1/500 dilution) in respective culture media. After staining, cells were washed once and resuspended in PBS+2.5% FBS and analyzed by flow cytometry.

BD sorters FACSAria II, FACSAria III and FACSAria FUSION; and BD analyzers FACSCelesta were used.

Immunostaining analysis

Cells were spun onto Poly-L-Lysine-coated slides (200 xg, 10 min), fixed with 4% paraformaldehyde and permeabilized with 0.5% Triton before blocking (PBS, 10% FBS, 5% BSA). Slides were incubated with primary antibodies in blocking solution O/N at 4°C. Secondary antibodies were added in PBS, 0.025% Tween for 1.5 h at room temperature (RT). After washing, nuclei were stained with 1 μg/mL DAPI and slides were mounted (Fluoromount G). Single cell images were captured by a Zeiss LSM700 Confocal Microscope (oil, 63x/1.4NA, Zen 2012) and processed and analyzed with ImageJ/Fiji and FlowJo10. Antibody dilutions used are the following: LAMP-1 1/200; TFEB 1/50; MYC 1/100; TfR1 1/50; Cathepsin D 1/100.

Analysis of TFEB-MYC correlation in single cell immunostaining data: fluorescence intensities for LAMP1, nuclear DAPI, MYC, nuclear MYC, TFEB, and nuclear TFEB were normalized to 10,000 for each cell and subject to log transformation.

Time-lapse imaging

Time-lapse experiments were conducted at 37°C, 5% O_2, 5%CO_2 on μ-slide $VI^{0.4}$ channel slides (IBIDI) coated with 20 μg/ml anti-human CD43-biotin antibody (Hilsenbeck et al., 2016). BFP^+ cells were sorted 3 days post-lentiviral transduction and cultured overnight in phenol red free IMDM supplemented with 20% BIT (StemCell Technologies, Inc.), 100 ng/mL human recombinant Stem Cell Factor (SCF), 50 ng/mL human recombinant Thrombopoietin (TPO), 100 ng/mL human Fms-related tyrosine kinase 3 ligand (Flt3L, all R&D Systems), 2 mM L-GlutaMAX (GIBCO), 100 U/mL penicillin and 100 μg/mL Streptomycin (GIBCO) before imaging. Brightfield images were acquired every 8 minutes for 3-4 days using a Nikon-Ti Eclipse equipped with a Hamamatsu Orca Flash 4.0 camera and a 10x CFI Plan Apochromat λ objective (NA 0.45). Single-cell tracking and fate assignment were performed using self-written software as previously described (Loeffler et al., 2019; Hilsenbeck et al., 2016, 2017). Time to division was calculated using R 3.5.3.

Cloning of lentiviral overexpression constructs

Lentiviral constructs expressing *TFEB* variants were constructed by Gateway™ cloning from pENTR223 donor plasmids into a lentiviral pRRL-based and Gateway™ adapted vector (pLBC2-BS-RFCA (Kaufmann et al., 2019)) downstream of a SFFV promoter and upstream of tagBFP driven by an EFS/SV40 chimeric promoter using the Gateway™ LR Clonase™ II Enzyme Mix according to manufacturer's instructions (Thermo Fisher). The original donor plasmid pENTR223-TFEB (HsCD00373101) was obtained from PlasmID (DF/HCC DNA Resource Core at Harvard Medical School). By standard site-directed PCR mutagenesis a STOP-codon was inserted (fw primer: 5′-TAG ACC CAG CTT TCT TGT ACA AAG TTG-3′; rev primer: 5′-TCA CAG CAC ATC GCC CTC C-3′) and subsequently pENTR223-TFEB-S142A (fw primer: 5′- CAC CCA TGG CCA TGC TGC AC-3′; rev primer: 5′- CAT TGG GAG CAC TGT TGC CAG C-3′) and pENTR223-TFEB- H240R_ I243N (fw primer: 5′- CGG AAC TTA AAT GAA AGG AGA CGA AGG-3′; rev primer: 5′- ATT GTC TTT CTT CTG CCG CTC C-3′) were generated using KOD Hot Start DNA Polymerase (Millipore-Sigma) followed by DpnI (NEB) digestion. The negative control (CTRL) vector for overexpression encodes *gp91phoxP415H* (catalytic inactive

Please cite this article in press as: García-Prat et al., TFEB-mediated endolysosomal activity controls human hematopoietic stem cell fate, Cell Stem Cell (2021), https://doi.org/10.1016/j.stem.2021.07.003

gp91phox/*CYBB*) that was previously cloned into the same lentiviral Gateway™ adapted vector (pLBC2-BS-RFCA; Kaufmann et al., 2019). MYC overexpressing vector was kindly provided by Linda Penn's lab.

Cloning of lentiviral knockdown constructs

The negative control (CTRL) vector for knockdown is a shRNA directed against Renilla luciferase (shCTRL) (Kaufmann et al., 2019). Additional shRNA sequences were predicted using the Sherwood algorithm as in Knott et al. (2014) and ordered as Ultramer DNA oligos (IDT). Subsequently, shRNAs were amplified using AmpliTaq Gold 360 Polymerase (ThermoFisher) using shRNA amplification Forward and Reverse primers. The PCR product was subsequently digested with BamH1 and Mlu1 and cloned into a UltramiR scaffold (miR30) within a pRRL-based vector downstream of a SFFV promoter and upstream stream of mCherry (pLBC2-mCherry).

shRenilla

TGCTGTTGACAGTGAGCGCAGGAATTATAATGCTTATCTATAGTGAAGCCACAGATGTATAGATAAGCATTATAATTCCTATGCCTAC
TGCCTCGGA

shTFEB-2

TGCTGTTGACAGTGAGCGAACGATGTCCTTGGCTACATCATAGTGAAGCCACAGATGTATGATGTAGCCAAGGACATCGTCTGCCT
ACTGCCTCGGA

shTFEB-3

TGCTGTTGACAGTGAGCGAGATGATGTCATTGACAACATATAGTGAAGCCACAGATGTATATGTTGTCAATGACATCATCCTGCCTA
CTGCCTCGGA

shTFEB-4

TGCTGTTGACAGTGAGCGCAGAAAGACAATCACAACTTAATAGTGAAGCCACAGATGTATTAAGTTGTGATTGTCTTTCTTTGCCTA
CTGCCTCGGA

shLAMP1

TGCTGTTGACAGTGAGCGATGGACGAGAACAGCATGCTGATAGTGAAGCCACAGATGTATCAGCATGCTGTTCTCGTCCAGTGCC
TACTGCCTCGGA

shTfR1

TGCTGTTGACAGTGAGCGCCAGCCAACTGCTTTCATTTGATAGTGAAGCCACAGATGTATCAAATGAAAGCAGTTGGCTGTTGCCT
ACTGCCTCGGA

Lentiviral Production and Transduction

VSV-G pseudotyped lentiviral vector particles were produced and titers were determined as

previously described (Kaufmann et al., 2019). Unless stated otherwise, after 16-20 hours of pre-stimulation in low cytokine media (see descriptioon below) cells were transduced with lentiviral vectors described above at matching multiplicity of infection (Kaufmann et al., 2019) aiming at mid-range (20%–40%) transduction efficiencies but without lentiviral preparation exceeding 20% of total culture volume. Transduction efficiency (%BFP$^+$ or %mCherry$^+$) was determined at day 3 post-transduction by flow cytometry on a BD Celesta, which served as initial input estimate for xenotransplantation assays.

Cell Culture

For *in vitro* experiments sorted cells were cultured in 96 well-plate round bottom with the indicated cell media.

- high cytokine media: StemPro-34 SFM media with the supplied supplement, 1x L-Glutamine, 1x Pen/Strep, 0.02% Human LDL and cytokines FLT3L (20 ng/mL), GMCSF (20 ng/mL), SCF (100 ng/mL), TPO (100 ng/mL), EPO (3 U/mL), IL-3 (10 ng/mL), IL-6 (50 ng/mL). This media was used to culture cells with the presence of DMSO, MYC inhibitor or BAF.
- low cytokine media: X-Vivo 10, 1% BSA, L-Glutamine, Pen/Strep and cytokines SCF (100 ng/ml), Flt3L (100 ng/ml), TPO (50 ng/ml) and IL7 (IL-7; 10 ng/ml). This media was used to transduce cells as indicated above.

For drug studies of untransduced cells, DMSO or MYC inhibitor (53.3 μM) were added at the time of seeding in high cytokine media and cells were harvested 4 days later for indicated analysis.

For drug studies of transduced cells, DMSO, MYC inhibitor (53.3 μM) or Bafilomycin (20 nM) were added in high cytokine media 1day after transduction with lentiviral vectors. Cells were harvested 4 days later for indicated analysis.

For lysosomal turnover studies, Bafilomycin (20 nM) or equivalent amount of DMSO was added to the cultures for 3 hours in StemPro-34 SFM media (1x L-Glutamine, 1x Pen/Strep, 0.02%) without cytokines.

Colony-Forming Cell Assays

For Lyso^H and Lyso^L cells

~20K LT-HSC were cultured for 4 days in high cytokine media and stained with LysoTracker as described above. For each group (based on LysoTracker fluorescence) 150 cells were sorted directly into 2 mL methylcellulose, supplemented with FLT3 Ligand (10 ng/mL) and IL6 (10 ng/mL) and plated onto 2x35 mm dishes as duplicates.

For transduced cells

At day 3 post-transduction, 150 LT-HSC BFP$^+$ or mCherry$^+$, 200 ST-HSC BFP$^+$, 300 MEP F1 BFP$^+$ or 300 MEP F2/3 BFP$^+$ cells were sorted directly into 2 mL methylcellulose, supplemented with FLT3 Ligand (10 ng/mL) and IL6 (10 ng/mL) and plated onto 2x35 mm dishes as duplicates.

Please cite this article in press as: García-Prat et al., TFEB-mediated endolysosomal activity controls human hematopoietic stem cell fate, Cell Stem Cell (2021), https://doi.org/10.1016/j.stem.2021.07.003

Colonies were allowed to differentiate for 10-11 days and then morphologically assessed in a blind fashion by a second investigator. Subsequently, colonies from replicate plates were pooled, resuspended in PBS/5% FBS and stained for flow cytometry analysis. For serial CFC assays, 0.5% of progeny from LT-HSC was added to fresh methylcellulose as above, replated and scored after 10-11 days.

Single-Cell Stromal Assays

Single cell *in vitro* assays were set up as described previously (Wagenblast et al., 2019; Itoh et al., 1989) with low passage murine MS-5 stroma cells (Mazurier et al., 2003) seeded at a density of 1500 cells per 96-well and grown for 2-4 days in H5100 media. One-day prior to coculture initiation, the H5100 media was removed and replaced with 100 μL erythro-myeloid differentiation media: StemPro-34 SFM media with the supplied supplement, 1x L-Glutamine, 1x Pen/Strep, 0.02% Human LDL and the following cytokines: FLT3L (20 ng/mL), GMCSF (20 ng/mL), SCF (100 ng/mL), TPO (100 ng/mL), EPO (3 U/mL), IL-2 (10 ng/mL), IL-3 (10 ng/mL), IL-6 (50 ng/mL), IL-7 (20 ng/mL), and IL-11 (50 ng/mL). Sorted single-cells were deposited in each well (80 wells/96-well plate). Colonies were scored after 15-17 days under the microscope and every individual well containing a visible colony was stained with antibodies listed in Table 1 and analyzed by flow cytometry using a BD FACSCelesta instrument equipped with a high throughput sampler (HTS).

Xenotransplantation

The progeny of 10K $CD34^+CD38^-$ transduced cells one day after transduction were intra-femoral injected in aged and gender matched 8-12 wk old male and female recipient NSG, NSG-SGM3 or NSG-W41 mice. At indicated time points, mice were euthanized, injected femur and other long bones (non-injected femur, tibiae) were flushed separately in Iscove's modified Dulbecco's medium (IMDM)+5%FBS and 5% of cells were analyzed for human chimerism along with BFP or mCherry and lineage specific markers . Sick and miss-injected mice were excluded from analysis. For purification of human cells from xenotransplanted mice, fresh or thawed BM from individual or from pools of 2-5 mice were mouse depleted (Mouse Cell Depletion Kit, Miltenyi) according to manufacturer's protocol and $CD45^+$/BFP^+ or $CD45^+$/$mCherry^+$ were sorted for serial transplantation by intra-femur injection in NSG-SGM3 mice at the indicated cell doses. A mouse was considered engrafted if % of human $CD45^+$ cells > 0.1. For LDA experiments LT-HSC frequency was estimated using the ELDA software (http://bioinf.wehi.edu.au/software/elda/) (Hu and Smyth, 2009).

For $Lyso^H$ and $Lyso^L$ LT-HSC: ~20K LT-HSC were cultured for 4 days in high cytokine media and stained with LysoTracker as described above. For each group (based on LysoTracker fluorescence) 1K LT-HSC were intra-femoral injected in aged and gender matched 8-12 wk old male and female recipient NSG-W41 or NSG-SGM3 mice and. Engraftment analysis of primary and secondary xenograft was performed as described above.

Quantitative RT-PCR for TFEB/LAMP1/TFRC knockdown and TFEB overexpression

In order to assess shRNA knock-down efficiency and gene overexpression, Nalm6 cells were infected at a multiplicity of infection of 0.3. Transduced cells were sorted for mCherry+ (knockdown) or BFP+ (overexpression) expression and total RNA was isolated and DNase treated using the RNeasy Micro Kit (QIAGEN, 74004) and cDNA was synthesized using SuperScript VILO (ThermoFisher, 11754050). qPCR was performed on the Roche Lightcycler 480 using SYBR Green (ThermoFisher, 4367659). All signals were quantified using the DCt method and were normalized to the levels of GAPDH.

qPCR primers:

TFEB
5′-ACCTGTCCGAGACCTATGGG-3′
5′-CGTCCAGACGCATAATGTTGTC-3′
LAMP1
5′-TCTCAGTGAACTACGACACCA-3′
5′-AGTGTATGTCCTCTTCCAAAAGC-3′
TFRC
5′-ACCATTGTCATATACCCGGTTCA-3′
5′-CAATAGCCCAAGTAGCCAATCAT-3′
GAPDH
5′-ACATCGCTCAGACACCATG-3′
5′-TGTAGTTGAGGTCAATGAAGGG-3′

RNA-seq processing and analysis

Freshly sorted populations from 3-5 independent CB pools or transduced cells *in vitro* after a second sort (PI^-BFP^+ or $PI^-mCherry^+$) on day 3 or 6 post-transduction were directly resuspended and frozen (−80°C) in PicoPure RNA Isolation Kit Extraction Buffer. RNA was isolated using the PicoPure RNA Isolation Kit (Thermo Fisher) according to manufacturer's instructions. Samples that passed quality control according to integrity (RIN > 8) and concentration as verified on a Bioanalyzer pico chip (Agilent Technologies) were subjected to further processing by the Center for Applied Genomics, Sick Kids Hospital: cDNA conversion was performed using SMART-Seq

v4 Ultra Low Input RNA Kit for Sequencing (Takara) and libraries were prepared using Nextera XT DNA Library Preparation Kit (Illumina). Equimolar quantities of libraries were pooled and sequenced with 4 cDNA libraries per lane on a High Throughput Run Mode Flowcell with v4 sequencing chemistry on the Illumina 30 HiSeq 2500 following manufacturer's protocol generating paired-end reads of 125-bp in length to reach depth of 55-75 million reads per sample. Reads were then aligned with STAR v2.5.2b (Dobin et al., 2013) against hg38 and annotated with ensembl v90. Default parameters were used except for the following: chimSegmentMin 12; chimJunctionOverhangMin 12; alignSJDBoverhangMin 10; alignMatesGapMax 100000; alignIntronMax 100000; chimSegmentReadGapMax parameter 3; alignSJstitchMismatchNmax 5 −1 5 5. Read counts were generated using HTSeq v0.7.2 (Anders et al., 2015) and general statistics were obtained from picard v2.6.0. Differential gene expression was performed using edgeR_3.24.3 following recommended practices. For the qLT-HSC versus aLT-HSC comparison (Table S1) the LT-HSC from the dataset GSE125345 were compared to the cultured CTRL LT-HSC from the TFEB-OE experiment. For the aLT-HSC versus aST-HSC comparison (Table S1), CTRL LT-HSC and ST-HSC from the TFEB-OE experiment were compared.

These data were used in a single sample gene set variation analysis using TFEB-OE and MYC-OE up and downregulated genes (top 100, 250 and 500 genes) using the gsva function of the R package GSVA_1.30.0.

Conditional Quantile Normalization (CQN) from the cqn R package was applied on TMM normalized raw counts in order to correct for gene length effect. Expression of TFEB, TFEC, TFE3 and MITF (GSE125345) was extracted from the data and plotted in each population using R stripchart.

Transcriptomic analysis of published datasets

GSE42414 (Laurenti et al., 2013)

Illumina HumanHT-12 beadchip expression data from lineage-depleted CB cells were downloaded from GEO. Normalized log2-transformed signal was used in a moderated t test in the R limma_3.38.3 package to compare HSC1 (Lin- CD34+ CD38- CD45RA- CD90+ CD49f+) and MPP Lin- CD34+ CD38- CD45RA- CD90- CD49f-). A rank file was obtained by ordering all genes using the t statistics from upregulated to downregulated genes in HSC1 compared to MPP and GSEA_4.0.3 was run using default parameters using the KEGG lysosome as gene-set.

Pathway enrichment analysis and visualization

Pathway enrichment analysis and visualization was performed as described previously (Reimand et al., 2019). Briefly, a score to rank genes from top upregulated to downregulated was calculated using the formula -sign(logFC) * -log10(pvalue). The rank file from each comparison was used in GSEA analysis (https://www.gsea-msigdb.org/gsea/index.jsp) using 2000 permutations and default parameters against indicated gene sets. All gene sets were obtained from a pathway database http://baderlab.org/GeneSets. EnrichmentMap version 3.1.0 in Cytoscape 3.7.0 was used to visualize enriched gene-sets with indicated FDR-q value and NES and a Jaccard coefficient set to 0.375. Full results in the comparison of CTRL versus TFEBWT-OE LT-HSC can be seen in Table S2. g:profiler (https://biit.cs.ut.ee/gprofiler/gost) was performed using the upregulated genes by TFEB-OE (FDRq-value $\leq$ 0.01), results can be seen in Table S2.

scRNA-seq Signature Enrichment

Using signatures derived from overexpression of TFEB and MYC in LT-HSCs (FDR < 0.05), we scored single CD34+CD38- HSPCs from three publicly available datasets for their relative expression of each signature. We then compared signature enrichment between cell cycle-primed HSPCs and non-primed HSPCs, as defined in Xie et al. (2019) The MYC OE signature was higher in the cycle-primed HSPCs while the TFEB OE signature was higher in the non-primed HSPCs, and these results were consistent across all three datasets (Velten et al., 2017, Pellin et al., 2019; van Galen et al., 2019)

Comparison of TFEB-regulated genes in MEP F2/3 with uncultured CB populations

The Gene Expression Omnibus dataset GSE125345 contains standardized RNA-Seq gene expression data of distinct hematopoietic cell states from uncultured cord blood. MEP, EryP, GMP, Gr, Mono and MEP populations were selected to be compared with the genes differentially expressed in $TFEB^{WT}$ versus CTRL MEP F2/3 cells. The top 250 genes enriched in MEP F2/3 $TFEB^{WT}$ and the top 250 genes enriched in MEP F2/3 CTRL were selected to be used as the reference signatures. First, bar graphs were created by selecting the MEP F2/3 $TFEB^{WT}$ reference signature, and calculating the number of scaled data that were above (> 0) or below (< 0) the mean for each population, corrected by the number of samples per population and 1,000 random permutations. Second, enrichment of both the $TFEB^{WT}$ and CTRL MEP F2/3 reference signatures were estimated in each sample of the uncultured cord blood population using ssgsea() from the GSVA_1.30.0 R package.

ATAC-seq processing and analysis

Transduced $BFP^{\pm}$ LT-HSC: Library preparation for ATAC-Seq was performed on 1000-5000 cells with Nextera DNA Sample Preparation kit (Illumina), according to previously reported protocol (Buenrostro et al., 2013). 4 ATAC-seq libraries were sequenced per lane in HiSeq 2500 System (Illumina) to generate paired-end 50-bp reads. Reads were mapped to hg38 using BWA (0.7.15) using default parameters (Li and Durbin, 2009). Duplicate reads, reads mapped to mitochondria, an ENCODE blacklisted region or an unspecified contig were removed ((ENCODE Project Consortium, 2012)). MACS (2.2.5) (Zhang et al., 2008) was used to call peaks in mapped reads. A catalog of all peaks was obtained by concatenating all peaks and merging any overlapping peaks. Peaks

Please cite this article in press as: García-Prat et al., TFEB-mediated endolysosomal activity controls human hematopoietic stem cell fate, Cell Stem Cell (2021), https://doi.org/10.1016/j.stem.2021.07.003

were considered unique to one condition or another if they were present in at least 2 out of three replicates but not in the contrasting condition. Homer (4.11.1) (Heinz et al., 2010) was used to calculate enrichment of subsets of peaks using default parameters plus the catalog of called peaks as background.

Chromatin Immunoprecipitation (ChiP)

For each immunoprecipitation, 50M hCB cells were crosslinked using 1% formaldehyde for 10 minutes at room temperature. Cells were lysed in modified RIPA buffer (0.1% SDS, 0.1% sodium deoxycholate, 1% Triton X-100, 140 mM NaCl, 1 mM EDTA, 10 mM Tris-HCl pH 8, supplemented with protease inhibitors (Roche). Crosslinked chromatin was sheared by sonication with the Bioruptor Pico (Diagenode) to 100-500 bp fragments (using 50-60 cycles, 30 s on/30 s off) and centrifuged to remove debris. Fragmented chromatin was incubated overnight at 4°C in 10-20 μg total target-specific antibody per ChIP; antibodies were pre-bound to a 1:1 mixture of Dynabeads Protein A and Dynabeads Protein G (Invitrogen). For TFEB, antibodies were pooled at indicated dilutions. Following overnight incubation, precipitated antibody-DNA complexes were washed sequentially with modified RIPA buffer, high salt modified RIPA buffer (modified RIPA buffer, 500 mM NaCl), LiCl buffer (1 mM EDTA, 250 mM LiCl, 0.5% NP-40, 0.1% sodium deoxycholate, 10 mM Tris-HCl pH 8), and TE buffer (10 mM Tris-HCl, 1 mM EDTA, pH 8), then resuspended in decrosslinking buffer (1% SDS, 0.1 M $NaHCO_3$). Complexes were decrosslinked for 6h at 65°C. DNA was extracted using Monarch PCR & DNA Cleanup kit (New England Biolabs) following manufacturer's protocol.

For quality control, quantitative real-time PCR was performed using SensiFast SYBR No-ROX kit (FroggaBio) on CFX96 Real-Time PCR Detection System (Bio-Rad). Primers against positive and negative control regions are listed in Rebuttal Table 2. Enrichment was normalized to 1% input.

For sequencing, DNA samples were quantified by Qubit; 2.5 ng DNA were used for library preparation using ThruPLEX DNA-seq kit (Takara Bio) according to the manufacturer's protocol.

Antibodies used for ChiP

Antibody	Target	Quantity per ChIP
2729S (Cell Signaling Technology)	IgG	10 μg
ab4729 (Abcam)	H3K27ac	10 μg
N262 (Penn lab)	c-Myc	20 μg
4240S (Cell Signaling Technology)	TFEB	1:400
D2O7D (Cell Signaling Technology)	TFEB	1:150
sc166736 (Santa Cruz Biotechnology)	TFEB	6 μg

ChiP-sequencing analysis

2 Replicates and associated inputs were aligned to hg38 using BWA with default paired-end parameters. All reads with quality score < 30, mitochondrial reads or reads mapping to an ENCODE blacklisted region were removed. MACS2 was used to call all peaks with a P value < 0.05 and IDR was used to combine the results from both replicates and identify 441 peaks of TFEB binding with an irreproducible discovery rate of < 0.05. 202 of these peaks were also identified in both TFEB ChiP-seq existing datasets. Promoters for genes identified in each category were identified and *lifted over from Refseq v19 to hg38*. Promoters were defined as the regions 2.5kb upstream to 0.5kb downstream of each TSS. 1000 permutations of an equal number of randomly selected and equivalently defined promoters were generated for each gene set, and the number of promoters which overlapped the TFEB peaks within each permutation was calculated as well as the observed enrichment for the real promoters and converted to Z-Scores.

QUANTIFICATION AND STATISTICAL ANALYSIS

GraphPad Prism was used for all statistical analysis except RNA-seq, ATAC-seq, microarray and single-cell RNA-seq datasets. Unless otherwise indicated, all individual values are shown on the graphs and statistical significance was determined by unpaired t test. *$p < 0.05$, **$p < 0.01$, ***$p < 0.001$ and ****$p < 0.0001$.